

SUSY Background to Neutral MSSM Higgs Boson Searches

B. FEIGL^{1*}, H. RZEHAKE^{2†} AND D. ZEPPENFELD^{1 ‡}

¹Institut für Theoretische Physik, Karlsruher Institut für Technologie
D-76128 Karlsruhe, Germany

²Physikalisches Institut, Albert-Ludwigs-Universität Freiburg, D-79104 Freiburg,
Germany

Abstract

Within the Minimal Supersymmetric Standard Model (MSSM) the production and decay of superpartners can give rise to backgrounds for Higgs boson searches. Here MSSM background processes to the vector boson fusion channel with the Higgs boson decaying into two tau leptons or two W-bosons are investigated, giving rise to dilepton plus missing transverse momentum signals of the Higgs boson. Starting from a scenario with relatively small masses of the supersymmetric (SUSY) particles, with concomitant large cross section of the background processes, one obtains a first conservative estimate of the background. Light chargino pair production plus two jets, lightest and next-to-lightest neutralino production plus two jets as well as slepton pair production plus two jets are identified as important contributions to the irreducible SUSY background. Light chargino and next-to-lightest neutralino production plus two jets and next-to-lightest neutralino pair production plus two jets give rise to reducible backgrounds, which can be larger than the irreducible ones in some scenarios. The relevant distributions are shown and additional cuts for MSSM background reduction are discussed. Extrapolation to larger squark masses is performed and shows that MSSM backgrounds are quite small for squark masses at the current exclusion limits.

*email: bastian.feigl @ kit.edu

†email: heidi.rzehak @ physik.uni-freiburg.de

‡email: dieter.zeppenfeld @ kit.edu

1 Introduction

One of the major tasks at the LHC is the search for Higgs bosons. In the Minimal Supersymmetric Standard Model (MSSM), for a wide range of parameters, one of the neutral Higgs bosons couples to vector bosons like a Standard Model Higgs boson i.e. with nearly no suppression of its coupling to gauge bosons with respect to the one in the Standard Model. For this Higgs boson, the search topologies of a Standard Model Higgs boson can be applied. The discovery potential for a MSSM Higgs boson at the LHC has been discussed in Refs. [1, 2].

A particularly interesting Higgs boson production channel is weak boson fusion (VBF, Fig. 1) which has been studied in [3] for the MSSM. The two tagging jets accompanying the VBF channel are an important characteristic allowing for sensitivity also at lower Higgs boson mass values. For $H \rightarrow WW$ and $H \rightarrow \tau\tau$ decay, yielding dilepton plus missing transverse momentum signatures, the major Standard Model background is due to processes like top quark pair production (plus jets), W boson pair production plus two jets, tau lepton pair production plus two jets, or Z boson production plus two jets.

In the MSSM, additional contributions to the background may arise from production of superpartners of the Standard Model type particles. In previous studies these background contributions have been taken into account in specific MSSM search channels where the Higgs boson is produced in supersymmetric (SUSY) cascade decays [1, 4, 5]. For Standard Model type processes SUSY background contributions have been discussed in the context of calibration processes [6]. However, first MSSM Higgs boson searches at the LHC did not include SUSY backgrounds [7, 8] (in the corresponding data analyses only the SM Higgs boson search topologies were used).

In this paper contributions from processes with SUSY particles to the background of the VBF Higgs boson production channel with subsequent Higgs boson decay into tau leptons or W bosons are investigated. For the produced tau leptons and W bosons the fully leptonic decay modes into electrons and muons are taken into account:

$$\begin{aligned} h &\rightarrow \tau^+\tau^- \rightarrow \ell^+\ell^- \nu_\ell \bar{\nu}_\ell \nu_\tau \bar{\nu}_\tau \\ h &\rightarrow W^+W^- \rightarrow \ell^+\ell^- \nu_\ell \bar{\nu}_\ell \end{aligned} \quad (1)$$

For searches of a relatively light MSSM Higgs boson (with mass around 120 GeV) the VBF production channel with a subsequent decay into tau leptons is one promising discovery channel [3] whereas the channel with a subsequent decay into W bosons is less important as a discovery channel but might be useful for measuring Higgs boson couplings [9].

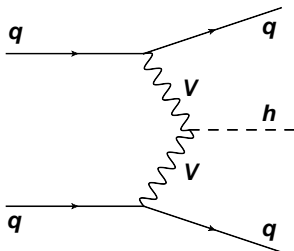


Figure 1: h production in weak boson fusion, with $V = W, Z$.

The final state of the signal processes is characterized by two charged leptons and missing energy from the decay of the Higgs boson, plus two jets from the scattered quarks. Background processes with SUSY particles can lead to the same final state topology and therefore contribute to the irreducible background: In the discussed scenarios, with the lightest neutralino as stable lightest supersymmetric particle (LSP), these background processes are chargino pair production plus two jets with subsequent decays of the charginos into a charged lepton, a lightest neutralino and neutrinos, lightest and next-to lightest neutralino production plus two jets where the next-to lightest neutralino decays into a charged lepton pair and a lightest neutralino as well as slepton pair production plus two jets with the sleptons decaying into charged leptons, lightest neutralinos and possibly neutrinos. Processes with other chargino and neutralino combinations, like next-to lightest neutralino pair production plus two jets or production of a chargino and a next-to lightest neutralino plus two jets, contribute to the reducible background. These processes give rise to additional jets or leptons which might be missed by the detector. The goal of this paper is an estimate whether the SUSY background is already sufficiently suppressed and therefore is of no concern in the Higgs boson analyses or whether further cuts have to be applied for a sufficient reduction of potential SUSY backgrounds. To reach this goal a conservative estimate of the SUSY background is helpful. Therefore, our starting point is a scenario with relatively small masses of the SUSY particles (though these masses are disfavoured by the current LHC exclusion limits [10, 11]). Since SUSY cross sections generally decrease with increasing squark mass, the low mass scenario provides an upper bound for SUSY backgrounds in a much larger range of scenarios. In a second step, larger, more realistic squark and gluino masses are considered and the resulting further reduction of the SUSY backgrounds is investigated.

While concerning the background only the Standard Model processes have been discussed in great detail [1–3, 9], the theoretical prediction of the VBF Higgs boson production cross section is known with a high accuracy in the Standard Model as well as in the MSSM: The next-to leading order (NLO) QCD contributions amount to about 10 % of the leading order cross section [12, 13]. The NLO electroweak corrections are of a similar size, about 5 – 10 % of the leading order cross section [13, 14]. Gluon induced contributions to the VBF channel have been investigated [15] and the interference effects of gluon and weak boson fusion have been studied [16]; both types of contributions have been found to be very small. Recently, approximate NNLO QCD corrections to VBF have been calculated and the theoretical uncertainty on the total cross section from higher order corrections and the uncertainties due to the parton distribution functions was estimated to be at the 2 % level each [17]. The NLO SUSY QCD corrections have found to be negligible [14, 18, 19] but also the NLO SUSY electroweak corrections are rather small, for a large part of the MSSM parameter space they are of the order of or even below 1 % of the leading order cross section [14, 19]. In special regions of the parameter space, especially for small SUSY masses [19] and in the non-decoupling region of the Higgs bosons [14], the corrections can be larger; in the latter case they can result in contributions up to 10 % of the leading order cross section. We will focus on a light MSSM Higgs boson in the decoupling region which means that it couples like a Standard Model Higgs boson to the gauge bosons.

Our paper is organized as follows: In Section 2 we present the different MSSM scenarios which we use in our analysis and list the processes which give rise to potentially significant SUSY backgrounds to VBF Higgs production in these scenarios. We discuss the tools used

in the analysis as well as parameters and approximations in Section 3. In Sections 4 and 5 we show our results for the irreducible and reducible SUSY backgrounds in a specific mSUGRA inspired scenario. The dependence on squark and gluino mass values is presented in Section 6. In Section 7 we focus on three other scenarios, one with light sleptons, another one with a very light LSP and a third one with small mass differences of the sparticles in the chargino decay chain. The situation for the 7 TeV LHC is discussed in Section 8. We conclude in Section 9.

2 The scenarios

We choose MSSM scenarios with the lightest neutralino χ_1^0 being the LSP, which is stable as we assume R-parity conservation. One widely considered parameter set within this class of MSSM scenarios is the SPS1a point [20], where the parameters are given at the GUT-scale in an mSUGRA type model and then evolved down to lower scales. The squark masses in the SPS1a scenario are relatively light which leads to higher production cross sections when squarks are involved. Therefore, this scenario is suited for finding an estimate of the upper bound of the SUSY contributions to the VBF background (note, however, that this is a very conservative estimate as the new measurements from ATLAS and CMS [10, 11] especially constrain scenarios with light squarks and gluinos with the exclusion bounds $m_{\tilde{q}} \approx m_{\tilde{q}} \gtrsim 800$ GeV). In the scenario that we choose as a starting point for our investigations, the values of the low scale parameters of the SPS1a scenario are used except for the one of the top trilinear coupling A_t . Instead, the low scale value of A_t is assumed as $A_t = -733$ GeV according to the m_h^{\max} scenario [21]. The new modified SPS1a scenario (SPS1amod) then has a lightest Higgs boson with a mass value of $m_h \approx 118$ GeV, which is above the LEP exclusion bound (the corresponding Higgs mass in the SPS1a scenario is slightly below the LEP exclusion bounds, $m_h \approx 112$ GeV). According to previous studies [1–3, 22] a lightest MSSM Higgs boson with the SPS1amod mass value is accessible via the VBF Higgs production channel with a subsequent decay into tau leptons. This holds also for a Standard Model like Higgs boson in the $h \rightarrow WW$ channel [23].

One further characteristic of the SPS1a point – which is preserved in our modified scenario – is that the branching ratio for the decay channel of a light tau slepton, $\tilde{\tau}_1$, into a tau lepton, τ , and a lightest neutralino is $BR(\tilde{\tau} \rightarrow \tau \chi_1^0) = 1$. The light charginos, χ_1^\pm , decay dominantly into a tau slepton and a corresponding neutrino, $\chi_1^\pm \rightarrow \tilde{\tau}_1^\pm \nu_\tau^{(\mp)}$. Furthermore, the second lightest neutralino decays only into two opposite charged leptons and a lightest neutralino, $BR(\chi_2^0 \rightarrow \ell^+ \ell^- \chi_1^0) = 1$, where the leptons ℓ include electrons, muons and tau leptons, $\ell = \{e, \mu, \tau\}$. The most important channels contributing to the irreducible background are

$$pp \rightarrow jj \chi_1^+ \chi_1^- \rightarrow jj \ell^+ \chi_1^0 \nu_\ell \ell^- \chi_1^0 \bar{\nu}_\ell \quad (2)$$

$$pp \rightarrow jj \chi_1^0 \chi_2^0 \rightarrow jj \chi_1^0 \ell^+ \ell^- \chi_1^0 \quad (3)$$

with $l = \{e, \mu, \tau\}$, see Sections 4.1 and 4.2.

Subleading contributions to the irreducible background in the SPS1amod scenario come from processes involving a direct slepton pair production accompanied by two jets with subsequent decays of the sleptons into corresponding leptons and invisible particles.

$$pp \rightarrow jj \tilde{e}_{L,R}^+ \tilde{e}_{L,R}^- \rightarrow jj \ell^+ \chi_1^0 \ell^- \chi_1^0 + \cancel{p}_T \quad (4)$$

$$pp \rightarrow jj \tilde{\mu}_{L,R}^+ \tilde{\mu}_{L,R}^- \rightarrow jj \ell^+ \chi_1^0 \ell^- \chi_1^0 + \cancel{p}_T \quad (5)$$

$$pp \rightarrow jj \tilde{\tau}_{1,2}^+ \tilde{\tau}_{1,2}^- \rightarrow jj \ell^+ \chi_1^0 \ell^- \chi_1^0 + \cancel{p}_T \quad (6)$$

While the \tilde{e}_R , $\tilde{\mu}_R$ and $\tilde{\tau}_1$ decay directly into the corresponding lepton and a neutralino, roughly a quarter of all \tilde{e}_L , $\tilde{\mu}_L$ and $\tilde{\tau}_2$ decay via a chargino which further decays, leading to further missing transverse momentum \cancel{p}_T . On the production level the $\tilde{\tau}_1$ pair production channel gives cross sections about 2 orders of magnitude smaller than the chargino and next-to-lightest neutralino production channels (14 fb with only very basic cuts (see jet cuts from Eq. (30)) compared to 2.6 pb for (2) and 1.4 pb for (3)). $\tilde{e}_{L,R}$ and $\tilde{\mu}_{L,R}$ pair production cross sections are of the same order as for the $\tilde{\tau}_1$ leptons within the SPS1amod scenario. However including the additional cuts from the Higgs boson analysis they increase the background by roughly 10% of the chargino / next-to-lightest neutralino background cross section. For higher squark and gluino masses the slepton contributions can become larger than the chargino and next-to-lightest neutralino channels (see Sections 4.3 and 6).

Several SUSY processes lead to a $\ell^+ \ell^- jj + \cancel{p}_T$ signature plus additional jets and leptons. As these additional particles might escape undetected, those processes contribute to the reducible background of VBF Higgs boson production. Details of our modeling of visible particles and our selection criteria are given in Section 5. In the SPS1amod scenario the dominant channels which contribute to the reducible background are:

$$pp \rightarrow jj \chi_1^+ \chi_2^0 \rightarrow jj \ell^+ \chi_1^0 \nu_\ell \ell^+ \ell^- \chi_1^0 \quad (7)$$

$$pp \rightarrow jj \chi_1^- \chi_2^0 \rightarrow jj \ell^- \chi_1^0 \bar{\nu}_\ell \ell^+ \ell^- \chi_1^0 \quad (8)$$

$$pp \rightarrow jj \chi_2^0 \chi_2^0 \rightarrow jj \ell^+ \ell^- \chi_1^0 \ell^+ \ell^- \chi_1^0 \quad (9)$$

More than two jets can occur from hadronic tau lepton or W boson decays. These processes contributing to the reducible background are discussed in detail in Section 5. We also look at several other processes that turn out to give only small contributions to the background. They are listed in Sections 3 and 5.4.

We use the program SUSYHIT 1.3 [24–27] for the evolution to lower scales with the default spectrum calculator SuSpect [26] (changing to the spectrum calculator SPHeno 3.0.beta [28] gives comparable results with only slight differences as expected). The resulting values are fed into the program FeynHiggs 2.6.5 [29] for precise values of the Higgs boson masses. The corresponding SLHA output file [30] is used as an input for the further calculations. As Standard Model input parameters in the spectrum calculator we take

$$\begin{aligned} \alpha_{em}^{-1}(M_Z) &= 127.934 & G_F &= 1.16639 \cdot 10^{-5} \text{ GeV}^{-2} \\ \alpha_s(M_Z) &= 0.1172 & M_Z &= 91.187 \text{ GeV} \\ M_b(M_b) &= 4.25 \text{ GeV} & M_t &= 172.5 \text{ GeV} \end{aligned} \quad (10)$$

with the top quark mass value from [31].

For our analysis of the SUSY background to the VBF Higgs production channel with a subsequent decay into two W bosons, we also consider a further modified SPS1a scenario (SPS1amod2), where we aim for a higher Higgs mass. Therefore we increase the soft SUSY breaking parameter values in the top squark sector, $M_{q3L} = 881 \text{ GeV}$, $M_{tR} = 808 \text{ GeV}$ and $A_t = -1833 \text{ GeV}$, at the low scale. This leads to a Higgs boson mass of $m_h \approx 124 \text{ GeV}$.

As in the SPS1amod case, the chargino background channel is not changed when taking the modified scenarios instead of the original SPS1a scenario. However, the neutralino channel cross section is a bit reduced for SPS1amod2: The particle masses calculated with SUSYHIT [24] are higher order corrected and therefore the branching ratios of the next-to-lightest neutralino decay are changed towards a preference of a decay into tau leptons which leads to a decrease of the cross section due to the further decay of the tau leptons into muons and electrons.

As the first LHC results become public and start to put constraints on low squark and gluino masses [10, 11], it becomes even more important to study the mass dependence of the SUSY backgrounds. Therefore we look into a series of scenarios, where we modify the squark and gluino mass related soft SUSY breaking terms:

- For final states containing only quarks of the first and second generation, we modify M_{q_1L} , M_{q_2L} , M_{uR} , M_{dR} , M_{cR} and M_{sR} by a factor $(1 + \xi)$ with $0 \leq \xi \leq 2$. We also modify M_3 to ensure that the gluino is always heavier than the squarks. This leads to average squark masses from 553 to 1581 GeV.
- When there is at least one b-quark in the final state, the mass of the stop has a large impact on the cross section. So for this final state, we increase the parameters that influence the third generation squark masses M_{q_3L} , M_{tR} , M_{bR} , A_t , A_b and M_3 by a factor $(1 + \rho)$ with $0 \leq \rho \leq 1$.

We also check a scenario where all SUSY particle masses are raised by increasing M_0 . The other values are changed according to the SPS1a slope [20],

$$M_0 = -A_0 = 130 \text{ GeV}, \quad M_{\frac{1}{2}} = 2.5M_0. \quad (11)$$

The parameters A_t , $M_L^{\tilde{t}}$ and $M_R^{\tilde{t}}$ are changed analogous to the procedure in SPS1amod2 in order to stay within the m_h^{max} scenario [21]. The SUSY mass values are then about 30% higher than in the SPS1a scenario.

Moving further away from the mSUGRA restrictions, we also study scenarios with different slepton masses, where the stau is heavier than the selectron and the smuon ($m_{\tilde{\tau}_1} = 334.8 \text{ GeV}$, $m_{\tilde{e}_L} = m_{\tilde{\mu}_L} = 141.9 \text{ GeV}$). This is achieved by changing the low-energy SUSY breaking parameters M_{eL} , $M_{\mu L}$, $M_{\tau L}$ and $M_{\tau R}$. For these slepton masses, we look at two scenarios with different squark masses corresponding to $\xi = 0$ and $\xi = 1.0$. These scenarios lead to an increased number of leptons in the final state, as the dominant decay chain no longer involves tau leptons, but directly first and second generation (s)leptons. So one decay with $BR(\tau \rightarrow \nu_\tau l \bar{\nu}_l) \approx 0.35$ with $l = \{e, \mu\}$ is avoided, which in addition leads to harder leptons.

Afterwards we check the influence of an almost massless LSP on our first scenario SPS1amod, where the stau mass is set to about half the value of the chargino mass. This is no longer a genuine MSSM scenario, but can illustrate the effect of the lepton hardness on our SUSY background processes.

Finally we illustrate the effect of two particles in the decay chain with a small mass difference. This is a mSUGRA scenario, where we again start with SPS1a and increase the trilinear coupling A_0 from -100 GeV to -750 GeV. This results in a small stau mass of 108 GeV, close to the mass of the LSP which is at 99.3 GeV.

	SPS1amod	$\xi = 1.0$	$\rho = 1.0$	SPS1a-slope	light sleptons
$m_{\tilde{u}_L} = m_{\tilde{c}_L}$	560.2 GeV	1090.9 GeV	576.1 GeV	713.7 GeV	560.1 GeV
$m_{\tilde{d}_L} = m_{\tilde{s}_L}$	565.6 GeV	1093.7 GeV	581.6 GeV	717.9 GeV	565.6 GeV
$m_{\tilde{u}_R} = m_{\tilde{c}_R}$	543.9 GeV	1055.4 GeV	559.6 GeV	691.4 GeV	543.9 GeV
$m_{\tilde{d}_R} = m_{\tilde{s}_R}$	543.6 GeV	1052.0 GeV	559.3 GeV	690.0 GeV	543.6 GeV
$m_{\tilde{b}_1}$	518.2 GeV	533.5 GeV	1003.6 GeV	685.8 GeV	518.2 GeV
$m_{\tilde{b}_2}$	544.9 GeV	560.4 GeV	1047.2 GeV	852.5 GeV	544.9 GeV
$m_{\tilde{t}_1}$	346.3 GeV	365.6 GeV	768.3 GeV	665.4 GeV	346.2 GeV
$m_{\tilde{t}_2}$	608.4 GeV	620.3 GeV	1060.0 GeV	976.1 GeV	608.4 GeV
$m_{\tilde{g}}$	607.6 GeV	1165.8 GeV	1140.7 GeV	783.6 GeV	607.6 GeV
$m_{\chi_1^+}$	181.1 GeV	183.8 GeV	182.0 GeV	244.6 GeV	180.2 GeV
$m_{\chi_2^0}$	181.6 GeV	184.4 GeV	182.5 GeV	244.9 GeV	180.8 GeV
$m_{\chi_1^0}$	97.5 GeV	98.1 GeV	97.6 GeV	129.9 GeV	97.1 GeV
$m_{\tilde{e}_L} = m_{\tilde{\mu}_L}$	199.7 GeV	199.6 GeV	199.6 GeV	256.1 GeV	141.9 GeV
$m_{\tilde{e}_R} = m_{\tilde{\mu}_R}$	142.6 GeV	142.6 GeV	142.7 GeV	181.7 GeV	142.6 GeV
$m_{\tilde{\tau}_1}$	133.0 GeV	133.1 GeV	132.8 GeV	172.9 GeV	334.8 GeV
$m_{\tilde{\tau}_2}$	203.9 GeV	203.8 GeV	204.1 GeV	259.1 GeV	397.4 GeV
m_h	118.2 GeV	118.4 GeV	122.7 GeV	124.0 GeV	118.2 GeV

Table 1: Particle masses in the scenarios SPS1amod, with higher first and second generation squark masses ($\xi = 1.0$), with higher stop masses ($\rho = 1.0$), SPS1a-slope and with light selectrons and smuons.

Some relevant SUSY particle masses and branching ratios in these scenarios are summarized in Tables 1 and 2.

3 The procedure

For our investigation we divide the processes in a production part with unstable SUSY particles in the final state and in a decay part which includes the decay chain of these SUSY particles. In the following we will describe the procedure and discuss its validity for the dominant irreducible background processes. The procedure is only slightly modified for the reducible background processes, these modifications are illustrated at the end of this section.

We use the program `MadGraph/MadEvent 4.4` [32] to generate parton level events with two jets and a pair of charginos or a lightest and next-to-lightest neutralino in the final state, respectively,

$$pp \rightarrow jj \chi_1^+ \chi_1^- , \quad (12)$$

$$pp \rightarrow jj \chi_1^0 \chi_2^0 \quad (13)$$

where p denotes the incoming protons with quarks of the first and second generation and gluons, $p = \{u, d, c, s, \bar{u}, \bar{d}, \bar{c}, \bar{s}, g\}$, and j is an outgoing jet at parton level, i.e. $j =$

	SPS1amod	$\xi = 1.0$	$\rho = 1.0$	SPS1a-slope	light sleptons
$BR(\tilde{u}_L \rightarrow \chi_1^+ d)$	65.0 %	62.9 %	65.1 %	65.1 %	65.0 %
$BR(\tilde{u}_L \rightarrow \chi_2^0 u)$	31.8 %	30.7 %	31.9 %	32.1 %	31.8 %
$BR(\tilde{u}_L \rightarrow \chi_1^0 u)$	0.7 %	0.6 %	0.7 %	1.0 %	0.7 %
$BR(\tilde{u}_R \rightarrow \chi_1^0 u)$	98.6 %	97.7 %	98.7 %	99.3 %	98.6 %
$BR(\tilde{t}_1 \rightarrow \chi_1^+ b)$	80.7 %	74.9 %	21.1 %	44.1 %	80.7 %
$BR(\tilde{b}_1 \rightarrow \chi_1^0 b)$	3.1 %	3.1 %	1.0 %	70.2 %	3.1 %
$BR(\tilde{b}_1 \rightarrow \chi_2^0 b)$	21.4 %	22.1 %	12.0 %	6.0 %	21.4 %
$BR(\tilde{b}_2 \rightarrow \chi_1^0 b)$	14.0 %	13.0 %	29.5 %	0.7 %	14.0 %
$BR(\tilde{b}_2 \rightarrow \chi_2^0 b)$	11.1 %	9.9 %	1.2 %	12.2 %	11.1 %
$BR(\chi_1^+ \rightarrow \tilde{\tau}_1^+ \nu_\tau)$	95.8 %	93.3 %	95.6 %	74.4 %	0.0 %
$BR(\chi_1^+ \rightarrow \ell^+ \tilde{\nu}_\ell)$	0.0 %	0.0 %	0.0 %	0.1 %	71.4 %
$BR(\chi_1^+ \rightarrow \tilde{\ell}_L^+ \nu_\ell)$	0.0 %	0.0 %	0.0 %	0.0 %	28.5 %
$BR(\chi_1^+ \rightarrow W^+ \chi_1^0)$	4.2 %	6.7 %	4.4 %	25.5 %	0.1 %
$BR(\chi_2^0 \rightarrow \tilde{\ell}_R^\pm \ell^\mp)$	11.9 %	12.3 %	10.6 %	8.1 %	0.4 %
$BR(\chi_2^0 \rightarrow \tilde{\ell}_L^\pm \ell^\mp)$	0.0 %	0.0 %	0.0 %	0.0 %	36.4 %
$BR(\chi_2^0 \rightarrow \tilde{\tau}_1^\pm \tau^\mp)$	88.1 %	87.0 %	89.4 %	87.3 %	0.0 %
$BR(\chi_2^0 \rightarrow \tilde{\nu}_\ell \bar{\nu}_\ell)$	0.0 %	0.2 %	0.0 %	0.3 %	63.2 %
$BR(\chi_2^0 \rightarrow \tilde{\nu}_\tau \bar{\nu}_\tau)$	0.0 %	0.5 %	0.0 %	0.8 %	0.0 %
$BR(\chi_2^0 \rightarrow \chi_1^0 Z)$	0.0 %	0.0 %	0.0 %	3.5 %	0.0 %
$BR(\tilde{\ell}_L^\pm \rightarrow \chi_1^0 \ell^\pm)$	63.7%	70.7%	66.1%	87.8%	100.0%
$BR(\tilde{\ell}_L^\pm \rightarrow \chi_1^\pm \nu_\ell)$	23.3%	18.8%	21.8%	8.0%	0.0%
$BR(\tilde{\ell}_R^\pm \rightarrow \chi_1^0 \ell^\pm)$	100.0%	100.0%	100.0%	100.0%	100.0%
$BR(\tilde{\tau}_1 \rightarrow \chi_1^0 \tau^\pm)$	100.0%	100.0%	100.0%	100.0%	94.0%
$BR(\tilde{\tau}_2 \rightarrow \chi_1^0 \tau^\pm)$	64.8%	70.4%	66.6%	85.8%	12.6%
$BR(\tilde{\tau}_2 \rightarrow \chi_1^\pm \nu_\tau)$	22.5%	19.0%	21.4%	9.3%	54.7%
$BR(h \rightarrow W^+ W^-)$	8.2%	8.3%	12.6%	15.1%	8.2%
$BR(h \rightarrow \tau^+ \tau^-)$	7.4%	7.4%	7.0%	6.7%	7.4%

Table 2: Branching ratios in the scenarios SPS1amod, with higher first and second generation squark masses ($\xi = 1.0$), with higher stop masses ($\rho = 1.0$), SPS1a-slope and with light selectrons and smuons. Here, $\tilde{\ell}^{(\sim)}$ means the combined (s)electron and (s)muon channel. The branching ratios of the \tilde{d} decays are comparable to the ones listed for \tilde{u} decays.

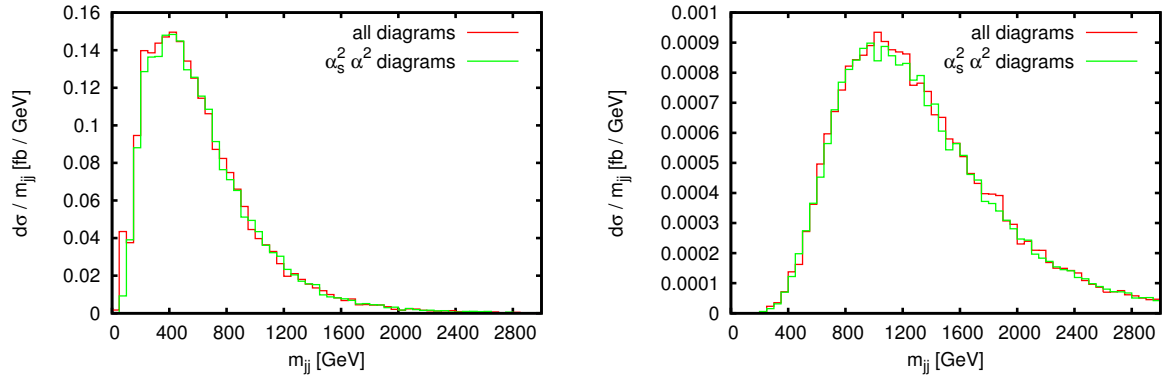


Figure 2: Comparison of full process vs. approximation for $\chi_2^0 \chi_1^0 jj$ production with minimal jet cuts (left) and an additional rapidity separation cut of $\Delta\eta \geq 4.2$ (right) in the dijet mass.

$\{u, d, c, s, \bar{u}, \bar{d}, \bar{c}, \bar{s}, g\}$. The slepton pair production processes

$$\begin{aligned}
 pp &\rightarrow jj \tilde{e}_{L,R}^+ \tilde{e}_{L,R}^-, \\
 pp &\rightarrow jj \tilde{\mu}_{L,R}^+ \tilde{\mu}_{L,R}^-, \\
 pp &\rightarrow jj \tilde{\tau}_{1,2}^+ \tilde{\tau}_{1,1}^-
 \end{aligned}
 \tag{14}$$

are generated with **MadGraph 5**, version 1.3 [33]. We abbreviate this process class by $\tilde{\ell}^+ \tilde{\ell}^- jj$ in the following. Final states containing at least one b-quark are generated separately. In this case we also allow b-quarks in the initial state. Contributions with at least one b-quark in the initial state, but none in the final state are very small and can be neglected. For all our calculations we use the parton distribution functions CTEQ611 [34]. Most parts of the analysis are done for a center of mass energy of 14 TeV at the LHC, but in Sect. 8 results for 7 TeV are shown.

We compare the $\chi_1^+ \chi_1^- jj$ and $\chi_2^0 \chi_1^0 jj$ cross sections to the ones generated with the program **Whizard 2.0** [35] and find agreement (see Fig. 6 for the comparison of the decay channels into stau leptons).

For the neutralino production we take only the contributions of $\mathcal{O}(\alpha_s^2 \alpha^2)$ into account. We checked that this is a reasonable approximation as the difference compared to the full process is very small. Furthermore events that we discard via this approximation show a very small rapidity separation between the tagging jets and have a small invariant jj mass. They would have been cut away by the requirement of a large rapidity separation for our signal processes (Fig. 2).

The $\mathcal{O}(\alpha_s^2 \alpha^2)$ contributions of the $\chi_1^0 \chi_2^0 jj$ production correspond to the squark production diagrams with a subsequent decay into neutralinos shown in Fig. 3. As those diagrams give the dominant contribution, the renormalization scale μ_R and the factorization scale μ_F are chosen of the order of the squark masses, which is $\mu_R = \mu_F = 550$ GeV for the SPS1amod and SPS1amod2 scenario.

In the case of the chargino production, however, not only the squark pair production diagrams contribute but also the other diagrams shown in Fig. 4. Relatively, these additional diagrams become even more important in the part of phase space which is interesting in the context of VBF backgrounds. For that reason, for the chargino production channel we choose

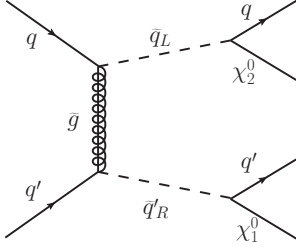


Figure 3: Dominant Feynman Graph for $\chi_1^0 \chi_2^0 jj$ production in SPS1amod scenario.

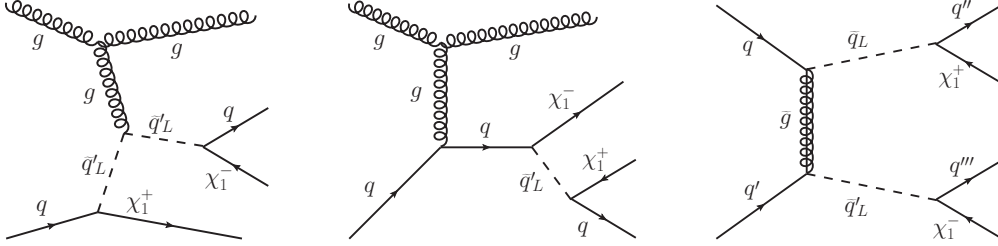


Figure 4: Dominant Feynman graphs for $\chi_1^+ \chi_1^- jj$ production in SPS1amod scenario.

the factorization scale as

$$\mu_F^2 = |p_T^{\text{jet}_1}| |p_T^{\text{jet}_2}| \quad (15)$$

and

$$\alpha_s^2 = \alpha_s(|p_T^{\text{jet}_1}|) \alpha_s(|p_T^{\text{jet}_2}|), \quad (16)$$

where $|p_T^{\text{jet}_i}|$ is the absolute value for the i -th jet (p_T ordered). With this choice we take into account the different scales of the event: for t-channel processes the jet p_T is the scale governing the momentum transfer between the QCD vertices, while for squark decays high p_T jets dominate and hence $p_T \approx m_{\tilde{q}}/2$ becomes the effective scale.

The relevant Feynman diagrams for the slepton pair production are shown in Fig. 5. Here no squarks are involved. Like in the chargino case, the transverse momentum of the two jets is the most relevant scale concerning the QCD part, so we use the same scale in the slepton production processes.

Concerning the scale uncertainty, we see the usual leading order α_s^2 scale dependence (listed in Table 3), which means that for a very precise analysis next-to leading order corrections would have to be taken into account. For some of the topologies in the relevant SUSY processes (e.g. the last diagram in Fig. 4), the K-factor on the total cross section is known [36, 37]. For SPS1amod and $\mu_R = \mu_F = m_{\tilde{q}}$, Prospino2 gives K-factors ranging from 1.25 for squark pair production up to 1.5 for squark-antisquark production. However, for some of the relevant topologies in our SUSY processes (e.g. the first two diagrams in Fig. 4), the NLO QCD corrections are not known, and therefore a scaling of the leading order results is not possible. The leading order scale variations of Table 3 cover the change due to known NLO corrections and we therefore do not attempt to correct for higher order effects. A full next-to leading order analysis is beyond the scope of this paper.

Due to the considered many particle final states and the large number of Feynman diagrams involved within the MSSM, a complete calculation of the cross sections including the

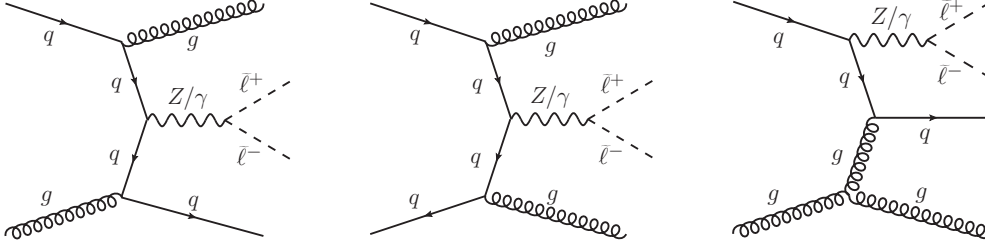


Figure 5: Dominant Feynman graphs for $\tilde{\ell}^+ \tilde{\ell}^- jj$ production in SPS1amod scenario.

full decay into leptons on matrix element level with programs like `MadGraph/MadEvent` [32] or `Whizard` [35] did not seem to be feasible. Instead, we feed the unweighted events produced with `MadGraph/MadEvent` into the Monte Carlo program `Herwig++ 2.4.2` [38] using Les Houches event files [39]. With `Herwig++` we simulate the subsequent χ_1^\pm , χ_2^0 and $\tilde{\ell}$ decays at parton level according to the branching ratios calculated by the spectrum generator (which is `SUSYHIT` in our case). Within the decay chains, `Herwig++` includes the spin correlations as described in [40], but we lose the spin information of the charginos and neutralinos at the interface between the two programs. To check the accuracy of this approximation, especially concerning spin effects, we consider the processes with the specific chargino decay chain

$$pp \rightarrow jj \chi_1^+ \chi_1^- \rightarrow jj \tilde{\tau}_1^+ \nu_\tau \tilde{\tau}_1^- \bar{\nu}_\tau \rightarrow jj \chi_1^0 \chi_1^0 \tau^- \bar{\nu}_\tau \tau^+ \nu_\tau \quad (17)$$

and neutralino decay chain

$$pp \rightarrow jj \chi_1^0 \chi_2^0 \rightarrow jj \chi_1^0 \tilde{\tau}_1^\pm \tau^\mp \rightarrow jj \chi_1^0 \chi_1^0 \tau^\pm \tau^\mp, \quad (18)$$

respectively, and perform the computation down to the $\tilde{\tau}$ -level using `MadGraph`. When the $\chi_1^\pm \rightarrow \tilde{\tau}^\pm \nu_\tau^{(-)}$ decay is included in the `MadGraph` calculation, the final state SUSY particles have spin-0. Therefore comparing the `MadGraph` result at this stage with the `MadGraph` result at the chargino level (`Herwig++` always computes the rest of the decay chain down to tau-lepton level) we get a good estimate on the impact of the chargino spin and of the spin of the second lightest neutralino on the distributions. We find that, for the charginos, the two different treatments of the $\chi_1^\pm \rightarrow \tilde{\tau}^\pm \nu_\tau^{(-)}$ decay agree very well. There are only small differences in the tau lepton p_T -distributions: While the p_T -distribution of the two tau leptons has the same shape for the chargino decay computed in `Herwig++`, there is a small asymmetry in the `MadGraph` case as can be seen in Fig. 6. For the neutralinos, the results

	$\zeta = 0.5$	$\zeta = 1.0$	$\zeta = 2.0$
$\chi_1^+ \chi_1^- jj$	1.71 fb	1.21 fb	0.88 fb
$\chi_2^0 \chi_1^0 jj$	1.37 fb	1.04 fb	0.82 fb
$\tilde{\ell}^+ \tilde{\ell}^- jj$	1.74 fb	1.23 fb	0.91 fb

Table 3: Scale dependence for $\chi_1^+ \chi_1^- jj$, $\chi_2^0 \chi_1^0 jj$ and $\tilde{\ell}^+ \tilde{\ell}^- jj$ cross sections with $\mu_R = \mu_F = \zeta \cdot \mu_0$ (basic jet and lepton cuts plus $\Delta\eta_{jj} \geq 4.2$ and $\eta_{j,min} \leq \eta_\ell \leq \eta_{j,max}$ are applied, see Eqs. (35), (36)).

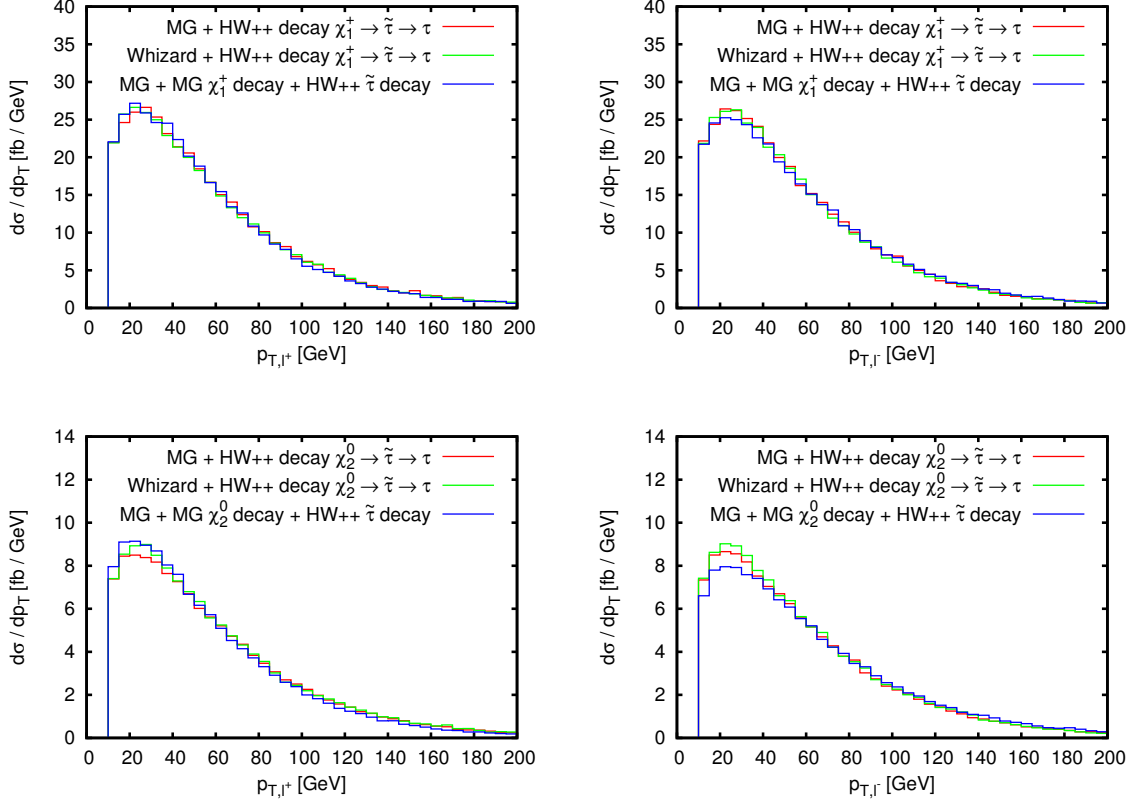


Figure 6: Comparison of MadGraph and Herwig++ performing the χ_1^\pm and χ_2^0 decay in the process from Eq. (17) and Eq. (18), respectively, with scales $\mu_F = \mu_R = M_Z$. The result of Whizard with the complete decay calculated by Herwig++ is also shown. The p_T distribution of the τ^+ is shown on the left, while the right plot shows the same for τ^- .

are similar; only the asymmetry in the p_T -distribution of the tau leptons, when the χ_2^0 decay is performed within the MadGraph calculation, is enhanced (see Fig. 6). As we use the same lepton cuts independent of the charge of the lepton and as we take into account all channels, particularly the $\tilde{\tau}^+$ and the $\tilde{\tau}^-$ channel in the neutralino case, neglecting the asymmetry still gives a reasonable result. Overall, these small effects in the chargino as well as in the neutralino case are negligible with respect to the accuracy of this leading order analysis.

For the SUSY processes which contribute to the reducible background of VBF Higgs boson production we again generate parton level events using MadGraph/MadEvent 4.4. The complete process list is:

$$pp \rightarrow j(j) \chi_1^\pm \chi_2^0, \quad (19) \qquad pp \rightarrow jj \chi_1^\pm \chi_2^\mp, \quad (24)$$

$$pp \rightarrow (j)(j) \chi_2^0 \chi_2^0, \quad (20) \qquad pp \rightarrow jj \chi_2^+ \chi_2^-, \quad (25)$$

$$pp \rightarrow jj \chi_3^0 \chi_1^0, \quad (21) \qquad pp \rightarrow jj \chi_2^\pm \chi_2^0, \quad (26)$$

$$pp \rightarrow jj \chi_4^0 \chi_1^0, \quad (22) \qquad pp \rightarrow jj \chi_2^+ \chi_1^0, \quad (27)$$

$$pp \rightarrow jj \chi_4^0 \chi_2^0, \quad (23) \qquad pp \rightarrow (j)(j) \tilde{g} \chi_1^0 \quad (28)$$

The processes of Eqs. (19) and (20) give by far the largest contributions and are discussed in more detail. A summary of the results for the other processes can be found in Section 5.4.

The topologies contributing to the cross section of these processes are similar to the ones of chargino pair production plus two jets (see Fig. 4), only for next-to lightest neutralino pair production plus two jets, Feynman diagrams with an initial squark pair production play a more important role. Therefore, we choose the dynamical factorization and renormalization scales analogously to Eqs. (15) and (16). The `MadEvent` events are again fed into `Herwig++`. But in contrast to the processes of the irreducible background, the hadronic decay modes of the tau lepton are needed as well: We have to model the contribution of soft hadronic tau lepton decays which escape detection, and take into account tau jets which are interpreted as tagging jets. For our analysis we construct a “partonic tau jet” by collecting all visible decay products of the `Herwig++` tau decay and combining their momenta to one single object. With this prescription, we treat every “tau jet” as a normal jet and give an upper bound on contributions containing hadronically decaying tau leptons. Further details on the event selection for the reducible background and our definition of visible objects will be given in Section 5.

For the generation of the signal processes we use the parton level Monte Carlo program `VBFNLO 2.6.2` [41] at leading order, as this program is very fast and efficient especially for the $h \rightarrow WW$ channel. The tau decay for $h \rightarrow \tau\tau$ is again done by `Herwig++`. The factorization and renormalization scales for the signal process are set to the momentum transfer of the exchanged W/Z boson between the quark lines.

We checked that detector effects from finite energy resolution for jets and leptons (modeled by a gaussian smearing) have only very small effects on our distributions, as they do not show any sharp peaks. Therefore we neglect them. One exception is the reconstructed tau pair mass of the $h \rightarrow \tau\tau$ signal, which is very sensitive to fake missing transverse energy. It can be parametrized by a Gaussian distribution [42] with

$$\sigma(E_x^{miss}, E_y^{miss}) = 0.41 \cdot \sqrt{\sum E_T}. \quad (29)$$

We therefore study the effects of (29) on the tau pair mass reconstruction. In the transverse energy E_T we include the energy deposit in calorimeters by hadronic parts of the event as well as contributions from the underlying event, but neglect pileup effects. From [43] we get an underlying event contribution to $\sum E_T$ of approximately 100 GeV for a center of mass energy $\sqrt{s} = 7$ TeV within the rapidity range $-4.5 \leq \eta \leq 4.5$. With a value of 33 GeV for $\sqrt{s} = 900$ GeV we extrapolate to an underlying event contribution of approximately 130 GeV at $\sqrt{s} = 14$ TeV.

4 SPS1a-like Scenario: Irreducible Background

Several SUSY processes contribute to the background of VBF Higgs boson production. We group them into two classes: Processes which match the signature of VBF Higgs boson production exactly and processes which produce additional jets or leptons. In this section we investigate the first class in detail, the other processes will be discussed in Section 5. We start with the processes containing charginos and neutralinos and continue with processes containing sleptons in Sect. 4.3.

First, we investigate the processes $pp \rightarrow jj\chi_1^+\chi_1^-$ and $pp \rightarrow jj\chi_2^0\chi_1^0$ including the subsequent decays of the charginos and neutralinos. These contributions to the background

mainly involve squarks and gluinos and their cross sections are relatively large when only minimal cuts are applied (see below and Fig. 7).

In principle the two Higgs decay channels $h \rightarrow \tau^+\tau^-$ and $h \rightarrow W^+W^-$ lead to the same signature in the detector, namely two hard jets with a large rapidity separation, two opposite charged leptons, and missing energy (from W or τ decay respectively). Therefore we have to consider the same processes as background. But as the signal processes feature different characteristics, we analyze them separately. Necessary cuts for Standard Model background reduction are partially taken from [2] in the case of $h \rightarrow \tau^+\tau^-$. For $h \rightarrow W^+W^-$ we follow [23], where this channel was discussed for relatively light Higgs boson masses.

4.1 χ_1^\pm and χ_2^0 Contributions to the $h \rightarrow \tau^+\tau^-$ Channel

With the procedure discussed in Section 3 and some minimal cuts on the produced jets and leptons which merely account for the detector acceptance

$$\begin{aligned}
p_{T,j} &\geq 20 \text{ GeV} & p_{T,\ell} &\geq 10 \text{ GeV} \\
|\eta_j| &\leq 4.5 & |\eta_\ell| &\leq 2.5 \\
R_{jj} &\geq 0.8 & R_{\ell\ell} &\geq 0.6 \\
R_{j\ell} &\geq 0.8, & &
\end{aligned} \tag{30}$$

we get background contributions from the two SUSY processes, which are very large compared to the signal. This is depicted in the left panel of Fig. 7 and Fig. 8. ($p_{T,P}$ denotes the transverse momentum of the particle P , η_P the rapidity of the particle P and $R_{P_1P_2}$ the R-separation of the particles P_1 and P_2 with $R_{P_1P_2} = (\Delta\eta_{P_1P_2}^2 + \phi_{P_1P_2}^2)^{1/2}$ where $\Delta\eta_{P_1P_2}$ is the rapidity separation of the particles P_1 and P_2 and $\phi_{P_1P_2}$ the azimuthal angle between those particles.) In the distribution of the rapidity separation between the two tagging jets, $\Delta\eta_{jj}$, but also in the distribution of the transverse momenta of the jets, the difference between the VBF signal and the SUSY backgrounds becomes clearly visible (see Fig. 7 and Fig. 8). The signal shows the typical VBF shape with two tagging jets in the forward and backward regions with a large rapidity separation and rather small transverse momenta of the jets. The background processes tend to have jets with smaller rapidity separation and larger transverse momenta which is the result of the jets being decay products of the produced SUSY particles. While for the hardest jet of the background processes the transverse momentum of the jet is larger than in the signal case the $\chi_1^+ \chi_1^- jj$ process shows two peaks in the transverse momentum distribution of the second jet, one for larger and one for small transverse momenta. This accounts for the different production mechanisms of the charginos: The peak at larger transverse momenta is due to squark pair production and decay (see right diagram in Fig. 4) while the peak at small transverse momenta is due to additional QCD radiation as can be seen in the two left diagrams in Fig. 4. Due to these differences, particularly in the $\Delta\eta_{jj}$ distribution, the additional cuts

$$\Delta\eta_{jj} \geq 4.2 \quad \eta_{j1} \cdot \eta_{j2} < 0 \quad \eta_{j,\min} \leq \eta_\ell \leq \eta_{j,\max} \tag{31}$$

improve the signal to background ratio tremendously, which is shown on the right panel of Fig. 7 and Fig. 8. Numbers for total cross sections at different cut levels are shown in Table 4.

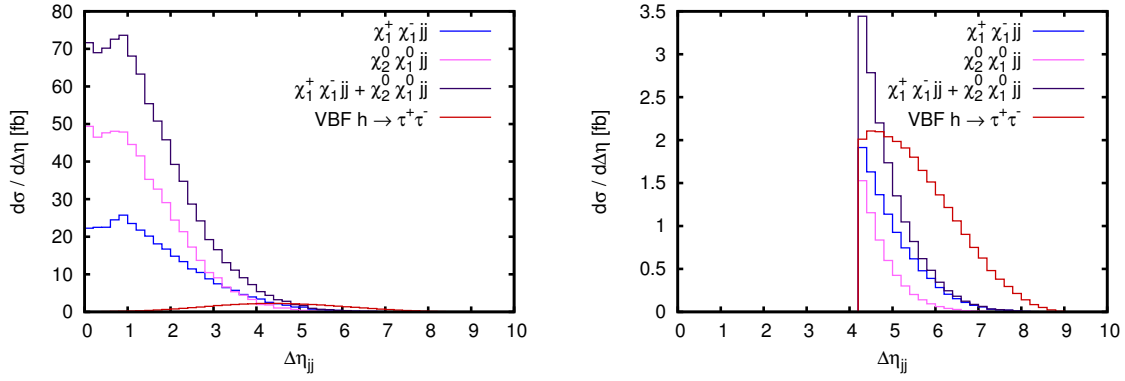


Figure 7: Rapidity separation for SUSY backgrounds and $h \rightarrow \tau\tau$ signal with basic cuts, Eq. (30), (left) and additional $\Delta\eta$ plus “leptons inside rapidity gap” cuts, Eq. (31) (right).

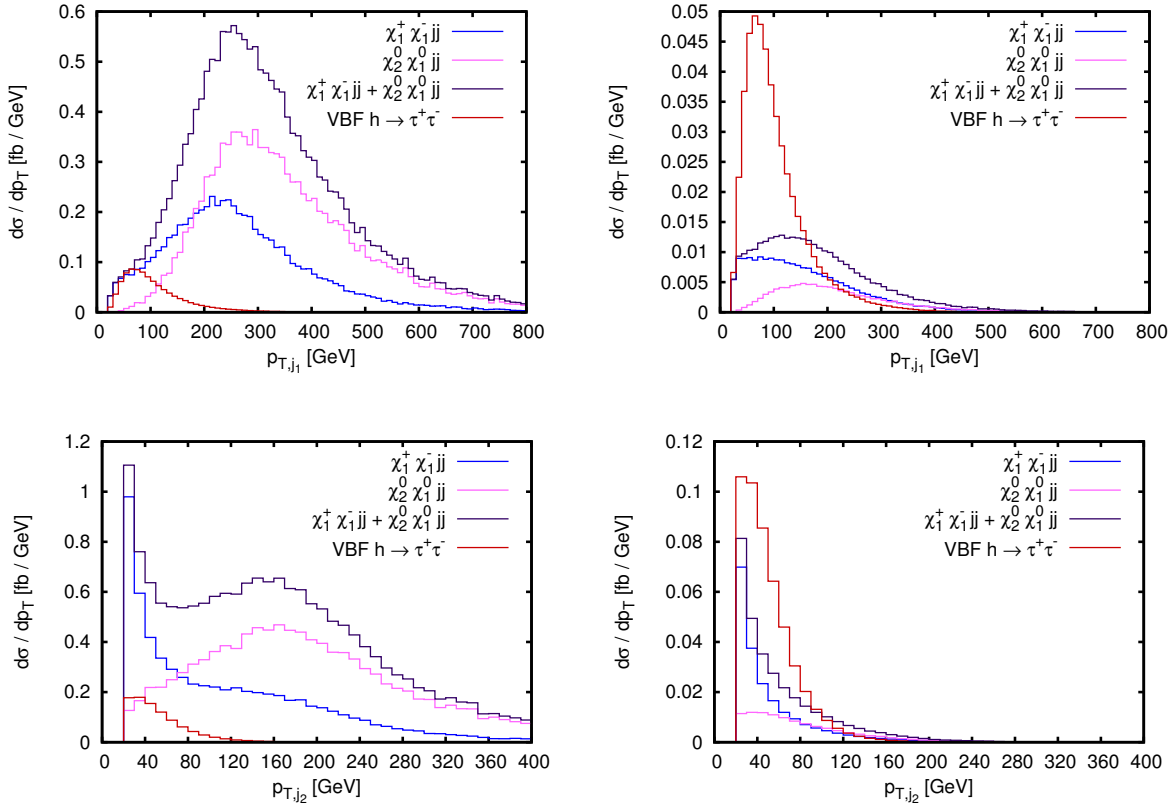


Figure 8: Transverse momentum of the harder (upper plots) and softer (lower plots) tagging jet for SUSY backgrounds and $h \rightarrow \tau\tau$ signal with basic cuts, Eq. (30), (left) and additional $\Delta\eta$ plus “leptons inside rapidity gap” cuts, Eq. (31) (right).

Further useful cuts for Standard Model background reduction which have been included in the analysis are a cut on the missing transverse momentum \cancel{p}_T and the jet pair mass m_{jj} .

$$\cancel{p}_T \geq 40 \text{ GeV} \quad m_{jj} \geq 700 \text{ GeV} . \quad (32)$$

The first one reduces backgrounds without neutrinos and improves the tau pair mass reconstruction [2]. The second cut helps reducing the QCD backgrounds [44]. With these cuts the combined cross section of $\chi_1^+ \chi_1^- jj$ and $\chi_2^0 \chi_1^0 jj$ production channels is roughly equal to the signal cross section.

An important technique to reduce Standard Model backgrounds in the $h \rightarrow \tau\tau$ channel is the reconstruction of the invariant tau pair mass $m_{\tau\tau}$, which corresponds to the Higgs boson mass, from the measured lepton four-momenta and missing energy [2, 45]. This geometrical reconstruction is possible, because the Higgs boson mass is much larger than the tau lepton mass m_τ , more precisely $m_h \gg 2 \cdot m_\tau$. This leads to highly boosted tau leptons. Therefore, to a good approximation, the tau leptons and their decay products are collinear in the lab frame and only the momentum fraction of the visible leptons compared to the tau leptons is needed for the reconstruction. As there is no other source of missing energy in the signal than from the tau decay, the two measured components of missing transverse energy can provide this information. The cuts

$$x_i \in [0, 1] \quad \cos \phi_{\ell\ell} \geq -0.9 \quad |m_{\tau\tau} - m_h| \leq 15 \text{ GeV} \quad (33)$$

can be used for the tau pair mass reconstruction. $x_i = p_{T,\ell_i}/p_{T,\tau_i}$ stands for the tau momentum fraction of the detected leptons, where $0 < x_i < 1$ is the physically allowed range. The cut on the azimuthal angle between the leptons discards events where the two leptons are back-to-back and therefore the reconstruction is not possible. The third cut accepts only events with a reconstructed mass around the expected Higgs mass. This is very effective for example against tau pairs from a Z -boson decay.

Processes involving SUSY particles in a R-parity conserving model always lead to additional missing transverse energy in the detector. Therefore these processes behave quite differently from the signal concerning the tau pair mass reconstruction as one can see in Fig. 9. The right plot of the Higgs signal shows the momentum fractions for the two leptons with the cuts of Eqs. (30) - (32), which is nicely located in the allowed range. The situation for the chargino background, and also for the one containing the next-to-lightest neutralino, is very different: For a large fraction of the events at least one of the x_i has a value below zero. The physically allowed events tend to have very small x_i . As the reconstructed tau pair mass is given by

$$m_{\tau\tau} = \frac{m_{\ell^+\ell^-}}{\sqrt{x_+ x_-}} , \quad (34)$$

these events yield a very high $m_{\tau\tau}$ and get sorted out by the “mass window” cut. We therefore improve the background suppression by more than a factor of 50 while the signal cross section reduction is only 8%. Missing E_T resolution from Eq. (29) slightly reduces the efficiency of the mass reconstruction for SUSY background suppression as they make the sharp signal resonance broader (see Fig. 10 and Table 4).

To summarize, we see that even when we include fake missing transverse momentum effects, the tau pair mass reconstruction is very efficient against SUSY processes: the additional sizable sources of missing transverse energy effectively eliminate the SUSY background.

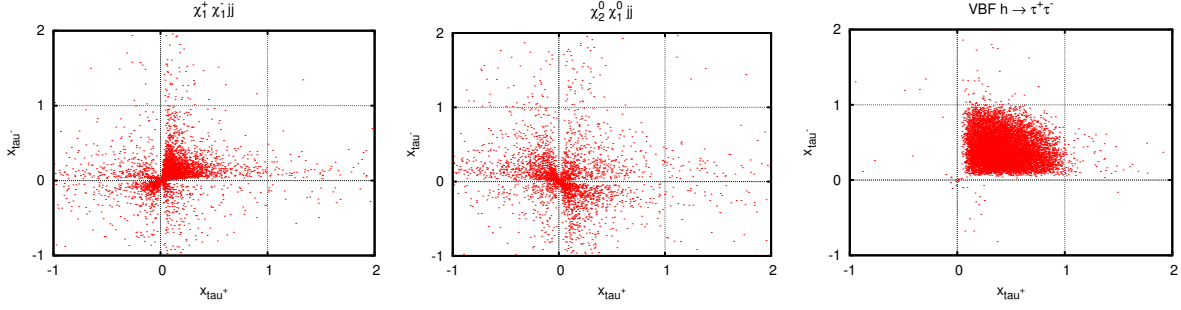


Figure 9: Tau momentum fractions for $\chi_1^+ \chi_1^- jj$, $\chi_2^0 \chi_1^0 jj$ and $h \rightarrow \tau\tau$ with cuts from Eqs. (30)-(32).

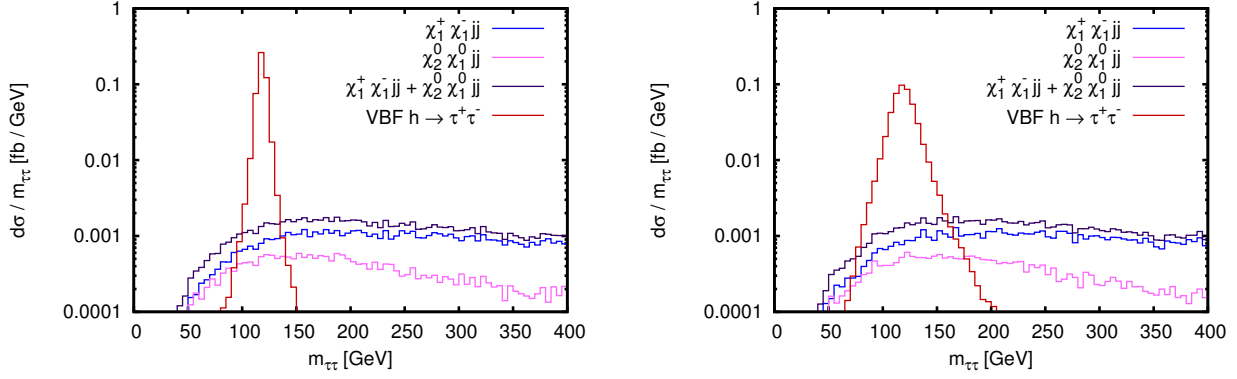


Figure 10: Reconstructed tau pair mass without the "mass window" cut from Eq. (33). The left panel is without detector effects, the plot on the right incorporates resolution effects according to Eq. (29).

Cuts	$\chi_1^+ \chi_1^- jj$	$\chi_2^0 \chi_1^0 jj$	VBF $h \rightarrow \tau\tau$
basics (Eq. (30))	64.13 fb	109.24 fb	9.17 fb
+ rapidity gap (Eq. (31))	2.04 fb	1.09 fb	4.94 fb
+ $\cancel{p}_{T,min}$ and m_{jj} (Eq. (32))	1.35 fb	0.96 fb	2.67 fb
+ $m_{\tau\tau}$ reconstruction (Eq. (33))	0.024 fb	0.015 fb	2.46 fb
+ fake \cancel{E}_T from Eq. (29)	0.025 fb	0.015 fb	1.93 fb

Table 4: Total cross sections for $\chi_1^+ \chi_1^- jj$, $\chi_2^0 \chi_1^0 jj$ and VBF $h \rightarrow \tau\tau$ at different cut levels.

4.2 χ_1^\pm and χ_2^0 Contributions to the $h \rightarrow W^+W^-$ Channel

4.2.1 Scenario SPS1amod

A full reconstruction of the invariant WW mass analogous to the τ decay mode of the previous section is not possible, because the W bosons are much heavier than the τ leptons and the collinear approximation does not work in this channel. Therefore we analyze this channel separately. We start with the basic cuts

$$\begin{aligned} p_{T,j} &\geq 20 \text{ GeV} & p_{T,\ell} &\geq 10 \text{ GeV} \\ |\eta_j| &\leq 4.5 & |\eta_\ell| &\leq 2.5 \\ R_{jj} &\geq 0.8 & R_{j\ell} &\geq 1.7 \\ m_{\ell\ell} &\geq 10 \text{ GeV} , \end{aligned} \tag{35}$$

where $m_{\ell\ell}$ is the lepton pair mass, and find a similar situation compared to the $h \rightarrow \tau\tau$ case with basic cuts, as we show in Table 5. Again, the cuts on the rapidity separation of the tagging jets are very efficient, here with an additional rapidity separation between jets and leptons which was already used for the SM background rejection in [23]:

$$\Delta\eta_{jj} \geq 4.2 \quad \eta_{j1} \cdot \eta_{j2} < 0 \quad \eta_{j,\min} + 0.6 \leq \eta_\ell \leq \eta_{j,\max} - 0.6 . \tag{36}$$

Several other cuts are needed for Standard Model background reduction [23] which also suppress the SUSY background relative to the signal:

$$\begin{aligned} \cancel{p}_T &\geq 30 \text{ GeV} & m_{jj} &\geq 600 \text{ GeV} \\ m_{\ell\ell} &\leq 60 \text{ GeV} & \phi_{\ell\ell} &\leq 140^\circ \\ m_{\tau\tau,\text{rec}} &\leq M_Z - 25 \text{ GeV} . \end{aligned} \tag{37}$$

The $m_{\tau\tau,\text{rec}}$ cut rejects all events where the tau pair mass reconstruction is possible ($x_+ > 0$ and $x_- > 0$) and the resulting reconstructed mass $m_{\tau\tau,\text{rec}}$ is greater than $M_Z - 25$ GeV, meaning they are consistent with $Z \rightarrow \tau\tau$. Especially the cuts on the azimuthal angle between the leptons $\phi_{\ell\ell}$ and the invariant mass $m_{\ell\ell}$ (see Fig. 11) improve the signal to SUSY background ratio. At this stage, the cross sections of $\chi_1^+\chi_1^-jj$ plus $\chi_2^0\chi_1^0jj$ are already suppressed by a factor of two compared to the vector boson fusion signal.

As mentioned before, the full WW mass reconstruction is not possible, but we can apply a cut on the transverse WW mass, which is effective against Standard Model backgrounds and the SUSY backgrounds. The transverse WW mass can be defined as [23]

$$M_T(WW) = \sqrt{(\cancel{E}_T + E_{T,\ell\ell})^2 - (\mathbf{p}_T + \mathbf{p}_{T,\ell\ell})^2} \tag{38}$$

with $E_{T,\ell\ell} = \sqrt{\mathbf{p}_{T,\ell\ell}^2 + m_{\ell\ell}^2}$ and $\cancel{E}_T = \sqrt{\mathbf{p}_T^2 + m_{\ell\ell}^2}$, where $\mathbf{p}_{T,\ell\ell}$ is the sum of the transverse momenta of the charged leptons. The signal peaks around the Higgs mass as depicted in Fig. 11. The cut

$$50 \text{ GeV} < M_T(WW) < m_h + 20 \text{ GeV} , \tag{39}$$

which was proposed in [23], reduces the chargino background by 25% and the next-to-lightest neutralino background by 75%, while the effect on the signal process is much smaller.

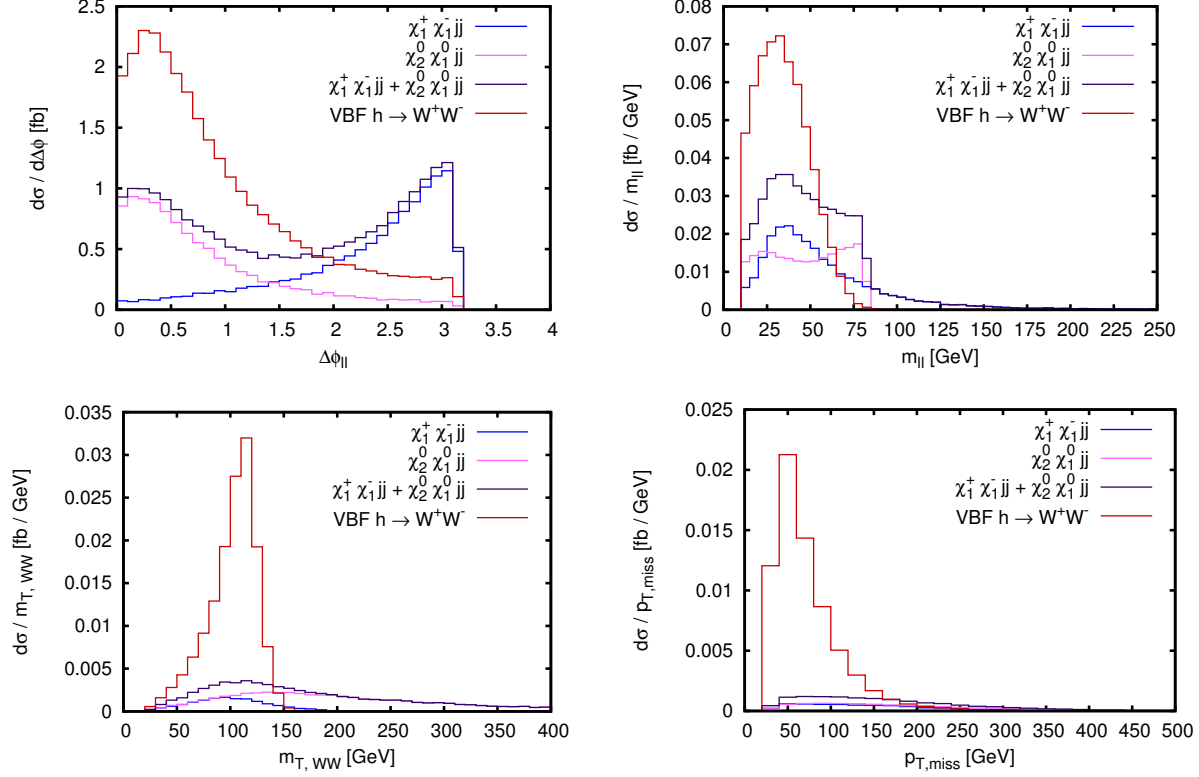


Figure 11: Upper row: Azimuthal angle between leptons (left) and invariant mass of both leptons (right) with cuts (35) - (36). Lower left panel: Transverse WW mass distribution with cuts (35) - (37). Lower right panel: \cancel{p}_T distribution with cuts (35) - (37), (39).

Cuts	$\chi_1^+ \chi_1^- jj$	$\chi_2^0 \chi_1^0 jj$	VBF $h \rightarrow WW$
basics (Eq. (35))	25.97 fb	66.79 fb	5.09 fb
+ rapidity gap (Eq. (36))	1.21 fb	1.04 fb	2.91 fb
+ $m_{jj}, m_{\ell\ell, max}, \dots$ (Eq. (37))	0.148 fb	0.537 fb	1.46 fb
+ $M_T(WW)$ (Eq. (39))	0.113 fb	0.146 fb	1.37 fb
+ $\cancel{p}_{T, max}$ (Eq. (40))	0.073 fb	0.081 fb	1.33 fb

Table 5: Total cross sections for $\chi_1^+ \chi_1^- jj$, $\chi_2^0 \chi_1^0 jj$ and VBF $h \rightarrow WW$ at different cut levels for the scenario SPS1amod.

Cuts	$\chi_1^+ \chi_1^- jj$	$\chi_2^0 \chi_1^0 jj$	VBF $h \rightarrow WW$
basics + rapidity gap (Eqs. (35)+(36))	1.20 fb	0.85 fb	4.96 fb
+ $m_{jj}, m_{\ell\ell, max}, \dots$ (Eq. (37))	0.149 fb	0.444 fb	2.48 fb
+ $M_T(WW)$ (Eq. (39))	0.110 fb	0.130 fb	2.28 fb
+ $\cancel{p}_{T, max}$ (Eq. (40))	0.070 fb	0.072 fb	2.21 fb

Table 6: Total cross sections for $\chi_1^+ \chi_1^- jj$, $\chi_2^0 \chi_1^0 jj$ and VBF $h \rightarrow WW$ at different cut levels for the scenario SPS1amod2.

Finally a cut on the missing transverse momentum improves the signal to background ratio significantly. As can be seen in Fig. 11, a cut of

$$\cancel{p}_T \leq 170 \text{ GeV} \quad (40)$$

leaves the signal almost unaffected, but reduces the background further by 40%. So after all cuts, the production of $\chi_1^+ \chi_1^- jj$ and $\chi_2^0 \chi_1^0 jj$ generate a background that accounts for 12% of the VBF $h \rightarrow W^+W^-$ cross section.

4.2.2 Scenario SPS1amod2 with a higher Higgs boson mass

We also checked the background with these cuts in the scenario SPS1amod2 introduced in Section 2, which aims for a higher Higgs boson mass. With $m_h = 124$ GeV compared to $m_h = 118$ GeV, the $h \rightarrow WW$ branching ratio and therefore the signal cross section is much higher. As can be seen in Table 6 the background due to the two SUSY processes amounts to only 6.4% of the signal cross section.

4.2.3 Central Jet Veto on Additional Jets from QCD Radiation

We now want to give a rough estimate for the efficiency of a central jet veto on the additional hadronic activity due to QCD radiation in SUSY backgrounds from Eqs. (2) and (3). Therefore we also generated events for the corresponding three-jet processes $\chi_1^+ \chi_1^- jjj$ and $\chi_2^0 \chi_1^0 jjj$ (in the latter case again in the approximation of taking only $\alpha_s^3 \alpha^2$ -diagrams into account). As the third jet in these processes typically arises from gluon radiation¹, the average multiplicity of additional jets can be estimated by $\bar{n} = \sigma(jjj)/\sigma(jj)$, which leads to the exponentiation model of Ref. [46]. In this model, with the final cuts from Eqs. (35) - (37), (39) - (40), we get the central jet veto probabilities $P_{veto} = 1 - \exp(-\bar{n})$ shown in Table 7. The three jet cross sections within the veto region are calculated with

$$\begin{aligned} p_{T,j_{veto}} &\geq 20 \text{ GeV} & \eta_{j_{tag,min}} &\leq \eta_{j_{veto}} \leq \eta_{j_{tag,max}} \\ R_{j_{tag,i},j_{veto}} &\geq 0.8 & R_{j_{veto},\ell} &\geq 0.3, \end{aligned} \quad (41)$$

where we require the two hardest jets to be the tagging jets $j_{tag,i}$ and consider the third jet j_{veto} as a veto candidate. In addition the final cuts of section 4.2.1 for the tagging jets and leptons are applied for the event generation. The small difference in the $h \rightarrow WW$

σ	jj	jjj	P_{veto}
$\chi_1^+ \chi_1^-$	0.073 fb	0.044 fb	0.45
$\chi_2^0 \chi_1^0$	0.081 fb	0.109 fb	0.74
$h \rightarrow WW$	1.38 fb	0.139 fb	0.10

Table 7: Total cross sections and central jet veto probabilities for $\chi_1^+ \chi_1^- jj(j)$, $\chi_2^0 \chi_1^0 jj(j)$ and $h \rightarrow WW$ with final cuts. For the jjj case, the cross sections are within the veto region from Eq. (41).

¹An exception is when gluino production is involved.

cross section compared to Table 5 is due to a different scale choice: We choose $\mu_F = \mu_R = \min(p_T(j_i))$ which is reasonable for the jj and jjj case. A detailed analysis of the central jet veto is beyond the scope of this paper, but we can see in the approximation of the exponentiation model, that a central jet veto would lead to a further reduction of the SUSY backgrounds.

Comparison of the cross sections with two and three additional jets in Table 7 also shows that the cross sections which we consider are sufficiently stable perturbatively. This situation is different from the one encountered in the $t\bar{t}$ background to the VBF Higgs search, where the $t\bar{t}j$ cross section strongly dominates over the $t\bar{t}$ cross section after final cuts [22].

4.2.4 Contributions from b-Quarks

As last task in this section, we want to investigate the contributions which arise when we allow for b-quarks to appear in the initial and final state. We separate this subprocess class into two subclasses: The first one requires at least one b/\bar{b} -quark in the initial state with no b/\bar{b} -quarks in the final state. Contributions from these subprocesses are checked to be very small and will be neglected. The more interesting subprocesses contain at least one b/\bar{b} -quark in the final state with no restrictions on the initial state. We call contributions from these subprocesses “contributions from b-quarks” in the following paragraphs.

For the chargino pair production, b-quark contributions with only basic cuts from Eq. (35) are of the same order as the previously discussed ones: Without b-quarks we have a total cross section of 26.0 fb (see Table 5), and b-quarks add 14.5 fb on top of this. The dominant b-quark contributions stem from the production of a \tilde{t}_1 pair with two gluons in the initial state where \tilde{t}_1 is the lighter top squark (Fig. 12) and account for more than 75% of the b-quark cross section. Because of the light \tilde{t}_1 -mass, compared to the other squark masses, the dijet mass of these events is much smaller than the one from non-b-contributions (see Fig. 13) and the rapidity separation of the two jets is also smaller. Therefore the cuts from Eqs. (36) and (37) are much more efficient. After applying all cuts (Eqs. (35) - (37), (39) - (40)) the b-quarks add only 25% to the chargino background. This can still be reduced by means of a b-jet veto. As b-quarks identified as tagging jets are widely separated in rapidity, they are unlikely to lie both in the central detector where the b-quark tagging is possible. Nevertheless as most of the b-jet contributions contain a $b\bar{b}$ pair, at least one of these quarks may lie in the central region of the detector. If we assume a b-tagging efficiency of

$$P_{\text{b-tag}} = 0.6 \quad \text{for} \quad |\eta_b| \leq 2.5, \quad (42)$$

we face a mistag rate of at most 1% [2,47]. We include this 1% mistag rate in our calculations. Vetoing events with at least one tagged b-quark, the b-quark contributions from charginos reduce to 13% of the chargino cross section without b-quarks for final cuts. Details are given in Table 8 and Fig. 13.

In contrast to the chargino production, squark production plays a minor role for the b-quark contributions to the $\chi_2^0\chi_1^0jj$ production. There are several reasons for this: First, the higher bottom squark mass compared to the small \tilde{t}_1 -mass. Second, the much smaller branching ratio of the decay channel bottom squark \tilde{b}_i , $i = 1, 2$ to bottom quarks and neutralinos. Also, the analogous Feynman graph to the dominant graphs of the chargino case is not allowed: Since a $g\text{-}\tilde{b}_1\text{-}\tilde{b}_2$ coupling does not exist, only $\tilde{b}_1 b_1$ and $\tilde{b}_2 b_2$ production

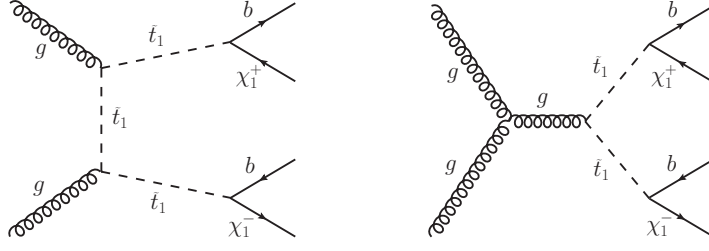


Figure 12: Dominant Feynman graphs for $\chi_1^+ \chi_1^- jj$ production with at least one b/\bar{b} quark in the final state.

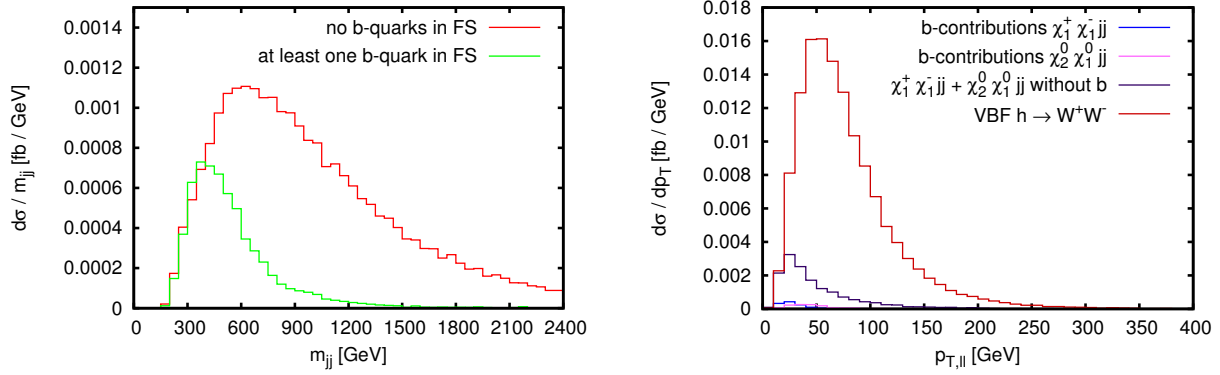


Figure 13: Left panel: Dijet mass distribution of $\chi_1^+ \chi_1^- jj$ with cuts (35) + (36). Right panel: Dilepton transverse momentum distribution with cuts (35) - (37), (39) - (40) and b-quark veto from Eq. (42).

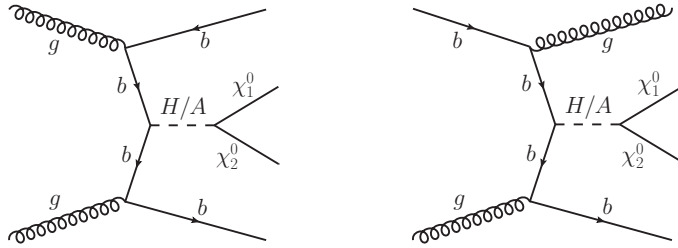


Figure 14: Additional Feynman graphs for $\chi_2^0 \chi_1^0 jj$ production with at least one b/\bar{b} quark in the final state.

Cuts	b-quark contr. in		no b-quarks	VBF
	$\chi_1^+ \chi_1^- jj$	$\chi_2^0 \chi_1^0 jj$	$\chi_1^+ \chi_1^- jj + \chi_2^0 \chi_1^0 jj$	$h \rightarrow WW$
Eq. (35)	14.50 fb	7.65 fb	92.76 fb	5.09 fb
+ Eq. (36)	0.31 fb	0.29 fb	2.25 fb	2.91 fb
+ Eqs. (37),(39),(40)	0.022 fb	0.022 fb	0.154 fb	1.33 fb
+ b-tagging (Eq. 42)	0.012 fb	0.014 fb	0.153 fb	1.32 fb

Table 8: b-quark contributions for $\chi_1^+ \chi_1^- jj$ & $\chi_2^0 \chi_1^0 jj$ in the scenario SPS1amod with different cuts and a b-quark veto.

needs to be considered. According to Table 2 their decay favors the production of either zero or two χ_2^0 states, whose decays do not typically result in exactly two charged leptons. Therefore the cross section is no longer dominated by squark pair production contributions, especially after the $\Delta\eta$ cut, and major contributions come from graphs like the ones shown in Fig. 14. As a consequence, we choose the factorization and renormalization scales as for the chargino production, described in Section 3. Detailed numbers are given in Table 8. In total, the b-quark contributions increase the SUSY background by 17% of the background due to chargino and next-to lightest neutralino production without b-quark contributions.

4.3 Backgrounds with Sleptons

Additionally to the background processes discussed in Sect. 4.1 and Sect. 4.2 there are further contributions to the background (already mentioned in Sect. 2 and Sect. 3) which involve the production of a slepton pair accompanied by two jets $pp \rightarrow \tilde{\ell}^+ \tilde{\ell}^- jj$, see Eq. (14). The cross section of this process compared to the production processes of charginos and neutralinos plus two jets is small, 85 fb for all slepton combinations versus 2.6 pb for the chargino production and 1.4 pb for the production of a lightest and a next-to-lightest neutralino (only the minimal jet cuts of Eq. (35) are applied). However, when taking into account the decays of the produced SUSY particles, the fraction of the slepton induced SUSY background becomes larger as the decay of \tilde{e}_R and $\tilde{\mu}_R$ produces directly detectable leptons. In contrast, the chargino and the next-to-lightest neutralino channels involve a cascade decay. Including the decays and again applying only the jet cuts of Eq. (35) the slepton channel cross section is 46 fb versus 312 fb and 321 fb for the cross section of the chargino and the neutralino channel, respectively.

Incorporating also the lepton cuts for the $h \rightarrow WW$ analysis, Eq. (35), the relative contribution of the sleptons rises again, see Table 9: The channels including the production and decay of \tilde{e}_R and $\tilde{\mu}_R$ do not contain a tau-lepton decay which leads to charged final state leptons with larger transverse momentum than in the case where the detected leptons originate from a tau-lepton decay. Therefore, with respect to the chargino and next-to-lightest neutralino case, the acceptance of the events is increased when the cut on the transverse momentum of the lepton is applied.

The rapidity separation of the jets, $\Delta\eta_{jj}$, is larger for the slepton channel than for chargino and next-to-lightest neutralino ones, which leads to a slepton channel cross section which is comparable in size to the ones of the chargino and the neutralino channel at the $\Delta\eta$ -cut level (see Fig. 15).

On the other hand the cut on the invariant jet pair mass is more efficient for the sleptons, as m_{jj} is rather small compared to the other channels which can be seen in Fig. 16. Also, the cut on the invariant lepton pair mass decreases the contribution of the slepton channel as the invariant lepton pair mass distribution is rather flat, yielding sizable contributions at larger masses (see Fig. 16).

Finally, the reconstructed transverse WW mass tends to be larger than for the signal which means that the corresponding cut is efficient in reducing this background contribution. Overall, taking all cuts into account, the cross section of the slepton channel is 0.028 fb whereas the cross section of the chargino and next-to-lightest neutralino channel including b-quark contributions is 0.179 fb. B-quark contributions to the slepton channel account for

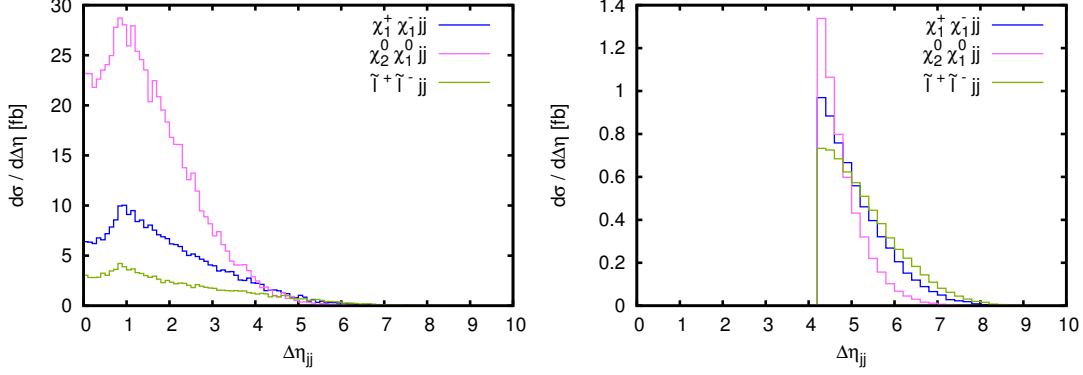


Figure 15: $\Delta\eta_{jj}$ distribution of the channels $\tilde{\ell}^+\tilde{\ell}^-jj$, $\chi_1^+\chi_1^-jj$ and $\chi_2^0\chi_1^0jj$ without b-quark contributions, applying the cuts of Eq. (35) (left) and of Eq. (35) and Eq. (36) (right).

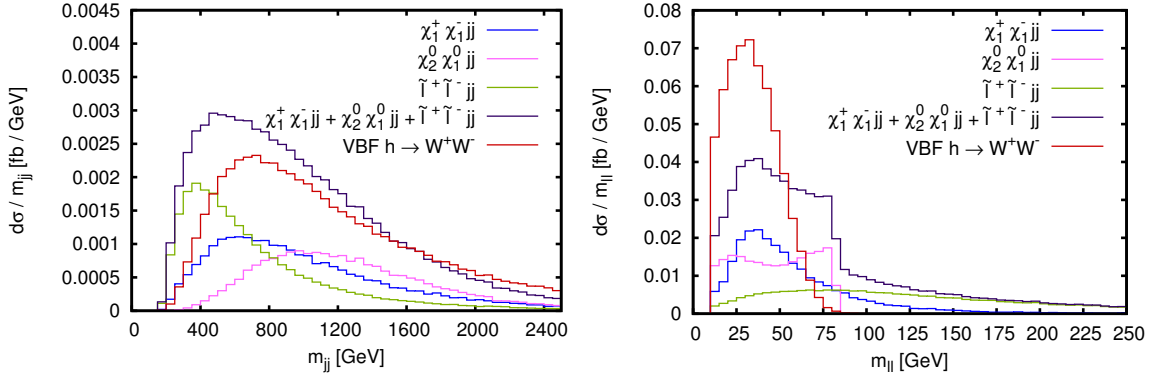


Figure 16: Invariant jet pair mass distribution (left) and invariant lepton pair mass distribution (right) of the $\tilde{\ell}^+\tilde{\ell}^-jj$, $\chi_1^+\chi_1^-jj$ and $\chi_2^0\chi_1^0jj$ background channel, of the sum of the considered background channels and the signal process. Cuts of Eq. (35) and (36) are applied, b-quark contributions are not included.

Cuts	$\chi_1^+\chi_1^-jj$	$\chi_2^0\chi_1^0jj$	$\tilde{\ell}^+\tilde{\ell}^-jj$	\sum_{irred}^{SUSY}	VBF $h \rightarrow WW$
Eq. (35)	40.47 fb	74.44 fb	11.55 fb	126.46 fb	5.09 fb
+ Eq. (36)	1.52 fb	1.33 fb	1.23 fb	4.08 fb	2.91 fb
+ Eq. (37)	0.177 fb	0.610 fb	0.080 fb	0.867 fb	1.46 fb
+ Eq. (39)	0.137 fb	0.172 fb	0.031 fb	0.340 fb	1.37 fb
+ Eq. (40)	0.095 fb	0.103 fb	0.028 fb	0.226 fb	1.33 fb
+ Eq. (42)	0.085 fb	0.094 fb	0.028 fb	0.207 fb	1.32 fb

Table 9: Total cross sections for $\chi_1^+\chi_1^-jj$, $\chi_2^0\chi_1^0jj$, $\tilde{\ell}^+\tilde{\ell}^-jj$ and VBF $h \rightarrow WW$ at various cut levels for the scenario SPS1amod, including b-quark contributions for $\chi_1^+\chi_1^-jj$ and $\chi_2^0\chi_1^0jj$.

only 3% of the corresponding cross section without b-quarks (including decays) in the final state and are therefore neglected. Summing the irreducible background contributions from the chargino, neutralino and slepton channels yields $\sigma_{irred}^{SUSY} = 0.207$ fb while the $h \rightarrow WW$ signal process has a cross section of $\sigma^{h \rightarrow WW} = 1.32$ fb.

For the $h \rightarrow \tau\tau$ analysis the situation is still very good: With all cuts of Eqs. (30)-(33), including detector effects of Eq. (29), the sleptons contribute with a cross section of 0.0034 fb, compared to 0.0274 fb and 0.0174 fb of the chargino and the next-to-lightest neutralino channel cross section (with b-quark contributions), respectively. Therefore the sum of these three processes ($\sigma_{irred}^{SUSY} = 0.048$ fb) is still much smaller than the $h \rightarrow \tau\tau$ cross section $\sigma^{h \rightarrow \tau\tau} = 1.93$ fb.

5 SPS1a-like Scenario: Reducible Background

In this section, we want to focus on processes that lead to additional jets or leptons compared to the signature of the considered VBF Higgs boson signal channels. In principle, these events can be eliminated by vetoing additional particles. However, these additional particles can remain undetected so that vetoing is not possible and the events contribute significantly to the SUSY background. At the beginning of this section, we will discuss the treatment of the additional particles. Then, the focus will be on the processes which dominantly contribute to the reducible background. In the last part of the section we will summarize the processes giving rise to the reducible and irreducible SUSY background for the considered VBF Higgs boson signal channels. The signal to SUSY background ratios will be given and the investigated processes that give only very small background contributions will also be listed.

5.1 Particle and Event Selection

Up to now, the particle selection of our parton level analysis was fairly simple: As, on parton level, the previously discussed processes produce exactly the same number of visible particles as appear in the final state of the signal processes, it was sufficient to apply some separation and p_T cuts for the matrix element calculation and to identify each particle with a detector signal. The analysis routine contained the other cuts which were used for the background suppression. This approach is no longer valid for the reducible background: For example, an additional tau lepton could decay hadronically and point into the same direction as a hard quark from the production process. Those two objects have to be considered as one jet.

For the new processes, we start again with some basic cuts on the jets applied already at `MadEvent` level ($p_{T,j} > 20$ GeV, $|\eta_{,j}| < 4.5$, $R_{jj} > 0.8$) which ensure a finite cross section. After performing the decay part with the help of `Herwig++`, the events contain up to two light partons generated already at `MadEvent` level plus leptons, additional jets (for example from tau lepton or W boson decay) and invisible particles from the decay of the SUSY particles.

The missing transverse momentum, \cancel{p}_T , is calculated via a vectorial sum of all particles that deposit their energy in the calorimeter: This includes light partons, tau jets and electrons up to $|\eta| \leq 4.5$ and muons up to $|\eta| \leq 2.5$. For all of these particles, a threshold p_T is applied, $p_T \geq 3$ GeV.

For the jet definition, we use the anti-kt jet clustering algorithm [48]. Leptons which are in the vicinity of a jet with $R_{jl} \leq 0.3$ are included into the jet. The resulting jets are defined as visible when they fulfill

$$p_{T,j} > 20 \text{ GeV}, \quad |\eta_j| < 4.5. \quad (43)$$

For the leptons, we require

$$p_{T,l} > 10 \text{ GeV}, \quad |\eta_l| < 2.5. \quad (44)$$

Events are kept when they finally have at least two visible jets and exactly one positively and one negatively charged visible lepton.

To get a well defined cross section, we have to discard an event, if it meets the following criteria:

- One of the jets generated at **MadEvent** level is not a tagging jet, but instead, a jet resulting from the following SUSY particle decay chain serves as tagging jet.
- A jet at **MadEvent** level has to be recombined with a jet originating from the further decays.

To explain the problems with events of this type it should be noted that the jets generated at **MadEvent** level can be characterized as two different kinds of jets, jets originating from a QCD splitting and jets produced via a decay of a heavy particle. These two contributions, however, can only be separated using a narrow width approximation but not in a calculation taking into account the full matrix elements as it is done in our approach:

- If the jet at **MadEvent** level originates from a QCD-splitting this event is part of the real emission contribution of the corresponding **MadEvent** level process with the number of jets reduced by one. This contribution is not IR safe but diverges for small p_T . Taking into account the virtual NLO corrections to the **MadEvent** level process with the number of jets reduced by one would yield an IR finite result. This means that the real emission contribution at parton-level is part of the NLO corrections. Another problem, going beyond the pure parton level, is that part of the real emission would be generated also by a parton shower and would lead to double counting.

In our approach, the IR divergences are regulated by the p_T cut of 20 GeV which is somewhat arbitrary but justified as long as the jets generated at **MadEvent** level are tagging jets and the parton-level process with exactly this number of jets is considered.

- The jet at **MadEvent** level can also be produced by the decay of a heavy particle. Recombined jets with the jet at **MadEvent** level being of this type are not fully included due to the p_T cut at **MadEvent** level. While the jet originating from the further cascade decays can have arbitrarily low values of p_T the jets at **MadEvent** level with low values of p_T , are not included.

Discarding events where the pure **MadEvent** level jets are no tagging jets leads to an error that can be approximated requiring $p_{T,j} > 20 \text{ GeV}$ for all jets and investigating how large the contribution of the discarded events is in that sample: In the first case, where a jet generated at **MadEvent** level is not a tagging jet, this contribution accounts for 1-3% of the

total cross section after applying the tagging jet rapidity separation cut used in the analysis. In the second case, where a jet originating from the `MadEvent` level process is recombined with a jet produced via the further decay chain, the size of the discarded contributions can be estimated to be below 1%. Considering the precision of our analysis, the overall size of the error due to the event selection described above is small.

After this procedure, the analysis cuts presented in the previous section are applied.

5.2 Contributions to the $h \rightarrow W^+W^-$ Channel

In this subsection, the dominant reducible background channels to the VBF Higgs production signal channel with a subsequent decay to W bosons are investigated. The considered channels comprise the production of a lightest chargino and a next-to lightest neutralino plus 2 jets as well as of a pair of next-to lightest neutralinos plus 2 jets including the subsequent decays of the SUSY particles, Eq. (7) - (9). Background channels with, at `MadEvent` level, the same SUSY particles but fewer jets in the final state play a much less important role and are listed, together with other less dominant channels, in Sect. 5.4.

In Table 10 the contributions of the different channels to the SUSY background are shown at different cut levels. The cuts of Eqs. (35) – (42) have been applied before to the irreducible background channels and, of course, have to be applied also to the reducible ones. As before, the typical VBF type cuts of Eq. (36) including the cut on the rapidity separation of the jets reduces the background considerably. The b-quark contributions to the $\chi_1^\pm \chi_2^0 jj$ channel are tiny, less than 1 % of the contributions without b quarks. As this is within the error originating from the Monte Carlo generation of the events these contributions are neglected.

Additionally to the cuts discussed before, a veto on additional visible jets as defined in Eq. (43) is applied,

$$\eta_{j_{tag},min} < \eta_{j_{decay}} < \eta_{j_{tag},max} \quad \text{with} \quad p_{T,j_{decay}} > 20 \text{ GeV}, \quad |\eta_{j_{decay}}| < 4.5. \quad (45)$$

It should be noted that due to the event selection as described in Sect. 5.1 this cut is only efficient on jets originating from the decay of a heavy particle. The central jet veto as described in Eq. (41), however, was used to reduce background events with extra jets from QCD radiation. It is clear that in an experimental analysis this discrimination between jets

Cuts	$\chi_1^+ \chi_2^0 jj$	$\chi_1^- \chi_2^0 jj$	$\chi_2^0 \chi_2^0 jj$		\sum_{red}^{SUSY}	VBF $h \rightarrow WW$
			no b	b-contr.		
Eq. (35)	100.8 fb	63.2 fb	46.4 fb	5.02 fb	215.4 fb	5.09 fb
+ Eq. (36)	3.94 fb	2.20 fb	1.35 fb	0.168 fb	7.66 fb	2.91 fb
+ Eq. (37)	1.46 fb	0.814 fb	0.537 fb	0.037 fb	2.85 fb	1.46 fb
+ Eq. (39)	0.562 fb	0.310 fb	0.231 fb	0.020 fb	1.123 fb	1.37 fb
+ Eq. (40)	0.406 fb	0.225 fb	0.150 fb	0.018 fb	0.799 fb	1.33 fb
+ Eq. (42)	0.403 fb	0.222 fb	0.149 fb	0.010 fb	0.784 fb	1.32 fb
+ Eq. (45)	0.275 fb	0.144 fb	0.059 fb	0.006 fb	0.484 fb	1.32 fb

Table 10: Total cross sections for $\chi_1^\pm \chi_2^0 jj$, $\chi_2^0 \chi_2^0 jj$ and VBF $h \rightarrow WW$ at different cut levels for the scenario SPS1amod.

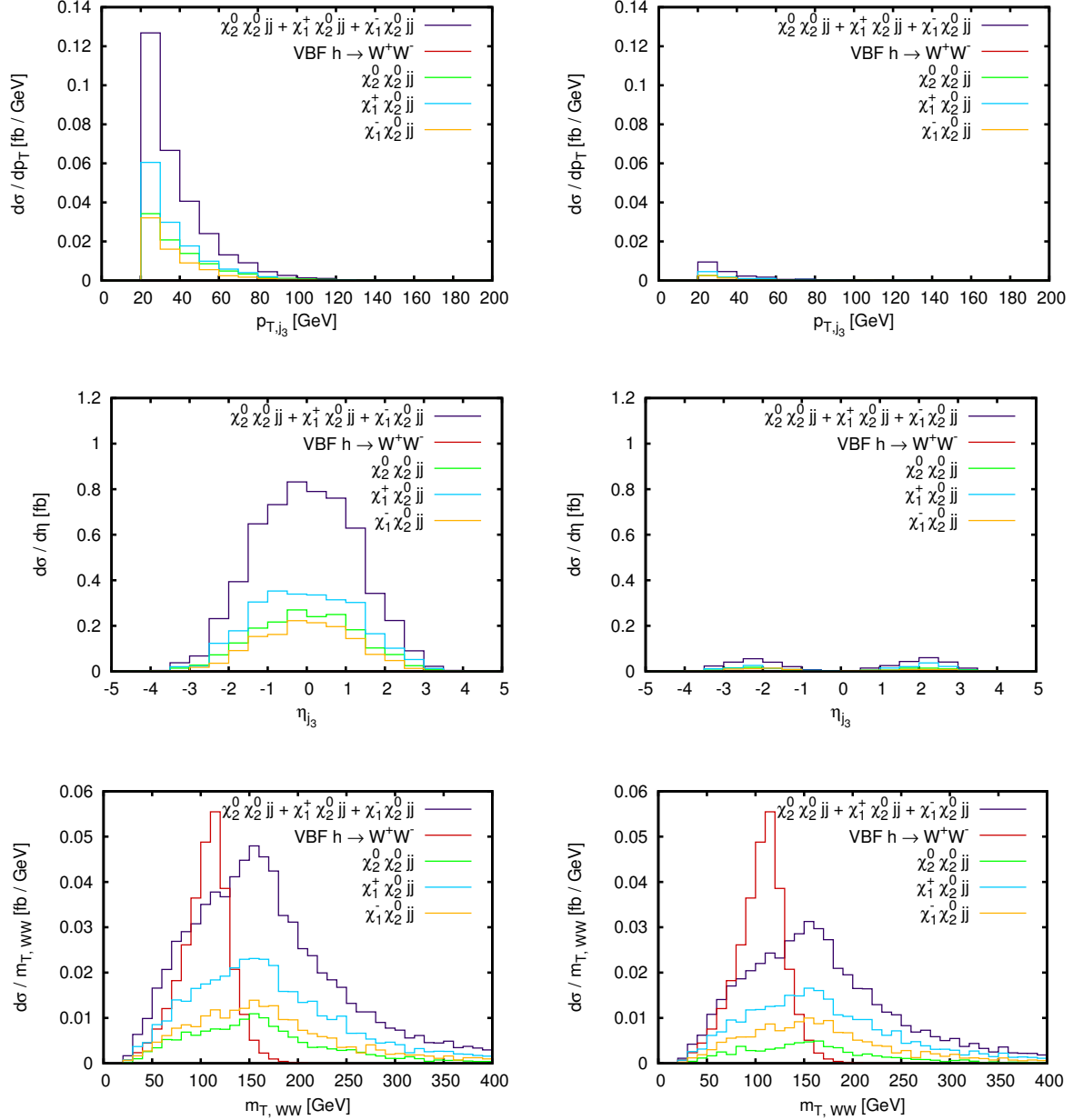


Figure 17: Transverse momentum (top row) and rapidity (middle row) of the third jet occurring in $\chi_1^\pm \chi_2^0 jj$ and $\chi_2^0 \chi_2^0 jj$. The bottom row shows the transverse WW mass distribution of these processes. Cuts for the left column are from Eqs. (35) - (36); the plots in the right column also include the veto from Eq. (45). Distributions are shown for the scenario SPS1amod.

from QCD radiation and from decays of heavy particles cannot be performed. This means that the central jet veto, Eq. (45), would also reduce the events with QCD radiation that we have neglected by our event selection from the beginning. In Fig. 17 the effect of the central jet veto, Eq. (45), is shown. On the left hand side, distributions with only basic and typical VBF cuts, Eq (35) and (36), are depicted while the ones presented on the right hand side include the central jet veto cut, Eq. (45). The p_T and η distribution of the third hardest visible jet show that the number of events with a third jet is efficiently reduced. In the last row, the distribution of the transverse WW mass is presented. The reducible SUSY background is efficiently reduced by the central jet veto, Eq. (45), especially in the case of the $\chi_2^0\chi_2^0jj$ channel, see also Table 10. However, this cut is not as efficient as it might appear by just considering the p_T and the η distribution of the third jet which is due to the events with no visible additional jets. Even after the central jet veto cut, the contribution of these channels to the SUSY background is larger than the one of the irreducible channels.

5.3 Contributions to the $h \rightarrow \tau^+\tau^-$ Channel

Considering the same background channels as in the subsection before, we now turn to the case of VBF Higgs boson production with a subsequent decay of the Higgs boson into τ leptons. The contributions of the channels to the SUSY background are listed in Table 11 for different cut levels. The first four cut levels, Eqs. (30) – (33), have also been applied in the analysis of the irreducible background channels. As before, using the tau mass reconstruction, Eq. (33), reduces the SUSY background very efficiently, leading to a much cleaner signal than in the case of the signal channel with a subsequent decay into W bosons. Taking into account the missing p_T resolution, Eq. (29), mainly affects the number of signal events as it leads to a broadening of the tau pair mass peak. Employing the central jet veto cut, Eq. (45), yields a further reduction of the background, in particular of the contribution of the $\chi_2^0\chi_2^0jj$ channel. Again, we have neglected the effect of the central jet veto on additional QCD radiation jets, which would lead to a further reduction of the cross section.

Overall, even after the central jet veto cut, the contribution of these reducible background channels is larger than the one coming from the irreducible ones. Due to the tau pair mass cut, however, the SUSY background contributions are still much smaller than the signal cross section.

Cuts	$\chi_1^+\chi_2^0jj$	$\chi_1^-\chi_2^0jj$	$\chi_2^0\chi_2^0jj$		\sum_{red}^{SUSY}	VBF $h \rightarrow \tau\tau$
			no b	b-contr.		
Eq. (30)	163.8 fb	104.4 fb	76.2 fb	9.22 fb	353.6 fb	9.17 fb
+ Eq. (31)	5.16 fb	2.81 fb	1.76 fb	0.228 fb	9.96 fb	4.94 fb
+ Eq. (32)	3.60 fb	1.90 fb	1.44 fb	0.080 fb	7.02 fb	2.67 fb
+ Eq. (33)	0.086 fb	0.047 fb	0.037 fb	0.002 fb	0.172 fb	2.46 fb
+ Eq. (29)	0.089 fb	0.046 fb	0.036 fb	0.002 fb	0.173 fb	1.93 fb
+ Eq. (45)	0.060 fb	0.033 fb	0.016 fb	0.001 fb	0.110 fb	1.93 fb

Table 11: Total cross sections for $\chi_1^\pm\chi_2^0jj$, $\chi_2^0\chi_2^0jj$ and VBF $h \rightarrow \tau\tau$ at different cut levels for the scenario SPS1amod.

5.4 Summary of Reducible and Irreducible Background

This subsection summarizes the results of Sections 4 and 5, which discussed the dominant SUSY background processes to the leptonic Higgs Boson channels $h \rightarrow WW$ and $h \rightarrow \tau\tau$ in vector boson production. Further sub-dominant processes are also listed and briefly discussed.

5.4.1 Contributions to the $h \rightarrow W^+W^-$ Channel

We investigated several SUSY particle production processes with subsequent decay of the SUSY particles in the scenario SPS1amod which can give rise to the same signature as the one of the $h \rightarrow WW$ channel in vector boson fusion. The complete list of processes is shown in Tables 12 and 13.

The processes from Table 12 give the largest contributions to the background and we discussed them in detail in the last sections. Figure 18 once again shows the distribution of the rapidity separation between the two hardest jets for the SUSY processes and the signal, once for only minimal cuts and once including the full set of cuts used in our analysis. With basic cuts, the SUSY background B^{SUSY} is larger by a factor of almost 70 compared to the signal process S . With all cuts except for the central jet veto on additional jets from SUSY particle decays, this factor is reduced and yields a signal of background ratio of

$$S/B^{SUSY} = 1.3, \quad (46)$$

where B^{SUSY} includes all processes listed in Table 12 from now on. Vetoing the additional jets from SUSY particle decays this ratio increases to

$$S/B^{SUSY} = 1.9. \quad (47)$$

In the experiment, a jet veto would also affect additional jets due to QCD radiation. We estimated this effect for the processes $\chi_1^+ \chi_1^- jj$ and $\chi_2^0 \chi_1^0 jj$ within the exponentiation model and found that the reduction for the SUSY processes is much larger than for the vector boson fusion process. Therefore we expect the signal to background ratio to improve further.

The processes with small contributions of Table 13 can be split into three classes:

- Processes of Table 12, but with fewer light jets at matrix element level
- Processes involving gluinos
- Processes with two jets at matrix element level and other chargino and neutralino combinations

In the first process class one (or two for $\chi_2^0 \chi_2^0$) of the tagging jets has to be created by a hadronic tau lepton decay, where the tau lepton comes from the decay of one of the charginos or neutralinos. These "one-jet" contributions are much smaller than the "two jet" contributions, because no resonant squark pair production is possible which produces fairly hard jets, while the tau jets are rather soft. Furthermore the rapidity separation between the hardest jets after the decay of the SUSY particles is smaller, increasing the efficiency of the rapidity gap cut of Eq. (36).

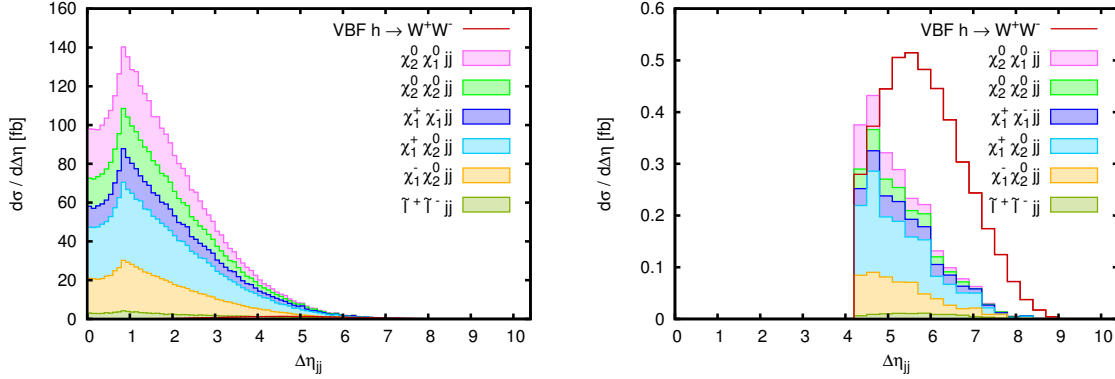


Figure 18: Rapidity separation for SUSY backgrounds and $h \rightarrow WW$ signal in the scenario SPS1amod. The left plot is for minimal cuts from Eq. (35). The right plot includes all discussed cuts from Eqs. (35) - (37), (39) - (40), (42), (45).

Processes	Cuts	basic Eq. (35)	+ rap. gap + (36)	+ $m_{inv}, \not{p}_T, \phi_{\ell\ell}, \text{b-tag}$ + (37), (39), (40), (42)	+ CJV on j_{decay} + (45)
$\chi_1^+ \chi_1^- jj$	no b	25.97 fb	1.21 fb	0.073 fb	0.073 fb
$\chi_1^+ \chi_1^- jj$	b-contr.	14.50 fb	0.31 fb	0.012 fb	0.012 fb
$\chi_2^0 \chi_1^0 jj$	no b	66.79 fb	1.04 fb	0.080 fb	0.080 fb
$\chi_2^0 \chi_1^0 jj$	b-contr.	7.65 fb	0.29 fb	0.014 fb	0.014 fb
$\tilde{\ell}^+ \tilde{\ell}^- jj$	no b	11.55 fb	1.23 fb	0.028 fb	0.028 fb
$\chi_1^+ \chi_2^0 jj$	no b	100.8 fb	3.94 fb	0.403 fb	0.275 fb
$\chi_1^- \chi_2^0 jj$	no b	63.22 fb	2.20 fb	0.222 fb	0.144 fb
$\chi_2^0 \chi_2^0 jj$	no b	46.40 fb	1.35 fb	0.149 fb	0.059 fb
$\chi_2^0 \chi_2^0 jj$	b-contr.	5.02 fb	0.168 fb	0.010 fb	0.006 fb
$\sum B^{SUSY}$		341.9 fb	11.74 fb	0.991 fb	0.700 fb
VBF $h \rightarrow WW$		5.09 fb	2.91 fb	1.32 fb	1.32 fb
S/B^{SUSY}		0.015	0.25	1.3	1.9

Table 12: Total cross sections of SUSY backgrounds dominant at low squark masses to the VBF $h \rightarrow WW$ channel for the scenario SPS1amod.

Processes	Cuts	basic Eq. (35)	+ rap. gap + (36)	+ $m_{inv}, \not{p}_T, \phi_{\ell\ell},$ b-tag + (37), (39), (40), (42)	+ CJV on j_{decay} + (45)
$\chi_1^+ \chi_2^0 j$	no b	15.96 fb	0.230 fb	0.008 fb	0.007 fb
$\chi_1^- \chi_2^0 j$	no b	8.93 fb	0.115 fb	0.004 fb	0.003 fb
$\chi_2^0 \chi_2^0 j$	no b	7.76 fb	0.052 fb	0.003 fb	0.002 fb
$\chi_2^0 \chi_2^0 j$	b-contr.	0.95 fb	0.010 fb	$\ll 0.001$ fb	$\ll 0.001$ fb
$\chi_2^0 \chi_2^0$	no b	0.25 fb	$\ll 0.001$ fb	$\ll 0.001$ fb	$\ll 0.001$ fb
$\chi_2^0 \chi_2^0$	b-contr.	0.15 fb	$\ll 0.001$ fb	$\ll 0.001$ fb	$\ll 0.001$ fb
$\tilde{g} \chi_1^0 jj$	no b	54.33 fb	3.15 fb	0.117 fb	< 0.01 fb
$\tilde{g} \chi_1^0 j$	no b	64.98 fb	0.54 fb	0.046 fb	0.007 fb
$\tilde{g} \chi_1^0$	no b	0.32 fb	$\ll 0.001$ fb	$\ll 0.001$ fb	$\ll 0.001$ fb
$\chi_1^+ \chi_2^- jj$	no b	2.03 fb	0.074 fb	0.003 fb	0.002 fb
$\chi_1^+ \chi_2^- jj$	b-contr.	0.67 fb	0.028 fb	< 0.001 fb	< 0.001 fb
$\chi_1^- \chi_2^+ jj$	no b	2.06 fb	0.095 fb	0.005 fb	0.003 fb
$\chi_1^- \chi_2^+ jj$	b-contr.	0.69 fb	0.029 fb	< 0.001 fb	< 0.001 fb
$\chi_2^+ \chi_2^- jj$	no b	0.27 fb	0.021 fb	< 0.001 fb	< 0.001 fb
$\chi_2^+ \chi_2^- jj$	b-contr.	0.11 fb	0.002 fb	$\ll 0.001$ fb	$\ll 0.001$ fb
$\chi_3^0 \chi_1^0 jj$	no b	0.33 fb	0.009 fb	< 0.001 fb	< 0.001 fb
$\chi_3^0 \chi_1^0 jj$	b-contr.	0.14 fb	0.002 fb	$\ll 0.001$ fb	$\ll 0.001$ fb
$\chi_4^0 \chi_1^0 jj$	no b	1.76 fb	0.041 fb	< 0.001 fb	< 0.001 fb
$\chi_4^0 \chi_1^0 jj$	b-contr.	0.24 fb	0.004 fb	$\ll 0.001$ fb	$\ll 0.001$ fb
$\chi_4^0 \chi_2^0 jj$	no b	2.40 fb	0.066 fb	0.005 fb	0.003 fb
$\chi_4^0 \chi_2^0 jj$	b-contr.	0.34 fb	0.003 fb	$\ll 0.001$ fb	$\ll 0.001$ fb
$\chi_2^+ \chi_2^0 jj$	no b	1.97 fb	0.061 fb	0.005 fb	0.002 fb
$\chi_2^+ \chi_2^0 jj$	b-contr.	0.06 fb	< 0.001 fb	$\ll 0.001$ fb	$\ll 0.001$ fb
$\chi_2^- \chi_2^0 jj$	no b	1.83 fb	0.041 fb	0.004 fb	0.002 fb
$\chi_2^- \chi_2^0 jj$	b-contr.	0.04 fb	< 0.001 fb	$\ll 0.001$ fb	$\ll 0.001$ fb
$\chi_2^+ \chi_1^0 jj$	no b	0.68 fb	0.013 fb	< 0.001 fb	< 0.001 fb
$\chi_2^+ \chi_1^0 jj$	b-contr.	0.01 fb	$\ll 0.001$ fb	$\ll 0.001$ fb	$\ll 0.001$ fb
\sum further processes		169.3 fb	4.59 fb	0.207 fb	< 0.048 fb

Table 13: Total cross sections of further SUSY backgrounds to the VBF $h \rightarrow WW$ channel for the scenario SPS1amod.

The production cross sections with minimal cuts are fairly large for the second process class, but the analysis cuts eliminate their contribution efficiently: For $\tilde{g}\chi_1^0$ the two jets of the gluino decay are very close in rapidity and no event survives the rapidity gap cut. For $\tilde{g}\chi_1^0 j$ and $\tilde{g}\chi_1^0 jj$ the tail of the tagging jet rapidity separation is still smaller than for the electroweak gaugino pair plus two jets processes. Another characteristic is the occurrence of additional hard jets from the gluino decay which can be well detected and vetoed.

The third class of processes involves mostly higher mass charginos and neutralinos with smaller production cross sections. Furthermore, due to their branching ratios a signature as the one of $h \rightarrow WW$ in vector boson fusion is not favoured.

5.4.2 Contributions to the $h \rightarrow \tau^+\tau^-$ Channel

For the $h \rightarrow \tau\tau$ analysis the same processes as before give the largest contributions to the SUSY background, see Table 14. The contributions from the processes listed in Table 13 are again much smaller, the sum of their contribution is listed in Table 14 as well.

SUSY backgrounds are much less troublesome in this search channel, due to the possibility to reconstruct the Higgs boson mass from the decay products. Therefore the overall signal to background ratio with all cuts is much higher than for $h \rightarrow WW$: It is

$$S/B^{SUSY} = 8.7 \quad (48)$$

Processes	Cuts	basic Eq. (30)	+ rap. gap + (31)	+ $m_{jj}, \cancel{p}_T, m_{\tau\tau}, \cancel{E}_{T,fake}$ + (32), (33), (29)	+ CJV on j_{decay} + (45)
$\chi_1^+ \chi_1^- jj$	no b	64.13 fb	2.04 fb	0.025 fb	0.025 fb
$\chi_1^+ \chi_1^- jj$	b-contr.	52.53 fb	0.47 fb	0.003 fb	0.003 fb
$\chi_2^0 \chi_1^0 jj$	no b	109.2 fb	1.09 fb	0.015 fb	0.015 fb
$\chi_2^0 \chi_1^0 jj$	b-contr.	12.88 fb	0.37 fb	0.003 fb	0.003 fb
$\tilde{\ell}^+ \tilde{\ell}^- jj$	no b	26.35 fb	1.89 fb	0.003 fb	0.003 fb
$\chi_1^+ \chi_2^0 jj$	no b	163.8 fb	5.16 fb	0.089 fb	0.060 fb
$\chi_1^- \chi_2^0 jj$	no b	104.4 fb	2.81 fb	0.046 fb	0.033 fb
$\chi_2^0 \chi_2^0 jj$	no b	76.15 fb	1.76 fb	0.036 fb	0.016 fb
$\chi_2^0 \chi_2^0 jj$	b-contr.	9.22 fb	0.23 fb	0.002 fb	0.001 fb
$\sum B^{SUSY}$		618.7 fb	15.82 fb	0.222 fb	0.159 fb
VBF $h \rightarrow \tau\tau$		9.17 fb	4.94 fb	1.93 fb	1.93 fb
S/B^{SUSY}		0.015	0.31	8.7	12
\sum further processes (see Table 13)		374.9 fb	6.41 fb	0.115 fb	< 0.016 fb

Table 14: Total cross sections of SUSY backgrounds dominant at low squark masses to the VBF $h \rightarrow \tau\tau$ channel for the scenario SPS1amod.

without a veto on additional jets from the SUSY particle decay, including the veto leads to

$$S/B^{SUSY} = 12. \quad (49)$$

6 Sparticle Mass Dependence

In this section we want to discuss the influence of larger sparticle masses on the SUSY background processes without changing the characteristic of our scenario which means that the branching ratios should only change slightly. In order to keep these characteristics, the gluino has to remain heavier than all squarks². As the gluino mass is only slightly larger than the squark masses, we have to increase it by the same factor as the squark masses.

The b-quark contributions involve mostly third generation squarks, while the other contributions have only first and second generation squark contributions. Therefore we check the b-quark contributions separately.

We focus on the dominant processes identified at the end of the previous section.

6.1 Squark + Gluino Mass Dependence

As described in Section 2, we vary the first and second generation squark masses and the gluino mass by scaling the low energy soft SUSY breaking terms M_{q_1L} , M_{q_2L} , M_{uR} , M_{dR} , M_{cR} , M_{sR} and M_3 by a factor $(1 + \xi)$, with $0 \leq \xi \leq 2$. Fig. 19 shows the cross section as a function of the average squark mass for two different sets of cuts: The left plot is for more inclusive cuts, taking only Eqs. (35) and (36) into account, while the right plot uses the full set of cuts Eqs. (35 – 37), (39), (40) and (45).

We see a strong suppression with higher squark and gluino masses of the processes containing two neutralinos. The decrease of the $\chi_2^0\chi_1^0jj$ cross section with increasing squark

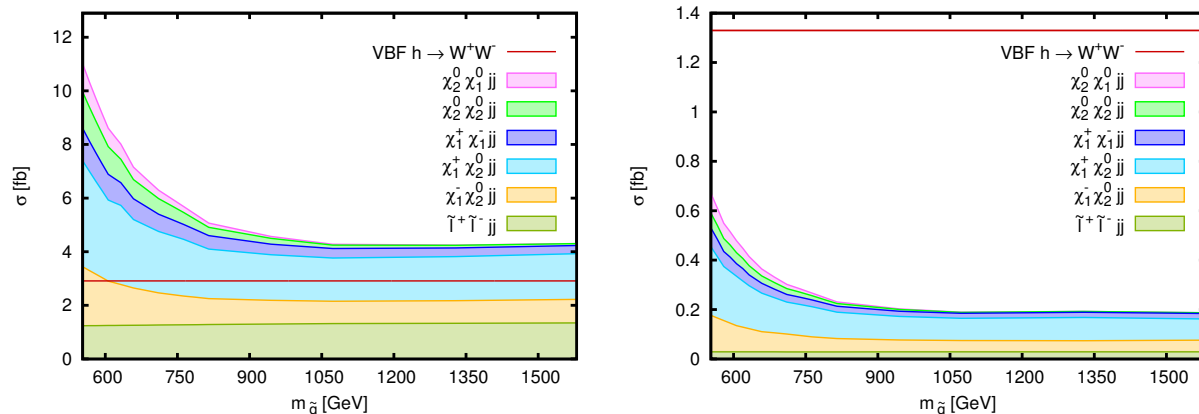


Figure 19: Squark+gluino mass dependence for the SUSY-backgrounds as a function of the average squark mass without b-quark contributions. Left panel: with cuts from Eqs. (35) + (36). Right panel: with additional cuts from Eqs. (37), (39), (40) and (45).

²If the gluino is lighter than the squarks with $m_{\tilde{g}} < m_{\tilde{q}} - m_q$, the decay channel $\tilde{q} \rightarrow q\tilde{g}$ will open up which, finally, does not lead to the considered final state.

Processes	Cuts	basic + rap. gap Eqs. (35) + (36)	+ $m_{inv} + \cancel{p}_T + \phi_{\ell\ell} + \text{b-tag}$ + (37), (39), (40), (42)	+ CJV on j_{decay} + (45)
$\chi_1^+ \chi_1^- jj$	no b	0.353 fb	0.020 fb	0.020 fb
$\chi_1^+ \chi_1^- jj$	b-contr.	0.227 fb	0.010 fb	0.010 fb
$\chi_2^0 \chi_1^0 jj$	no b	0.032 fb	0.001 fb	0.001 fb
$\chi_2^0 \chi_1^0 jj$	b-contr.	0.228 fb	0.010 fb	0.010 fb
$\tilde{\ell}^+ \tilde{\ell}^- jj$	no b	1.311 fb	0.028 fb	0.028 fb
$\chi_1^+ \chi_2^0 jj$	no b	1.611 fb	0.122 fb	0.090 fb
$\chi_1^- \chi_2^0 jj$	no b	0.836 fb	0.061 fb	0.046 fb
$\chi_2^0 \chi_2^0 jj$	no b	0.128 fb	0.011 fb	0.004 fb
$\chi_2^0 \chi_2^0 jj$	b-contr.	0.137 fb	0.008 fb	0.004 fb
$\sum B^{SUSY}$		4.86 fb	0.271 fb	0.213 fb
VBF $h \rightarrow WW$		2.91 fb	1.32 fb	1.32 fb
S/B^{SUSY}		0.60	4.9	6.2

Table 15: Total cross sections of SUSY backgrounds dominant at low squark masses to the VBF $h \rightarrow WW$ channel for average squark masses of 1.1 TeV.

Processes	Cuts	basic + rap. gap Eqs. (35) + (36)	+ $m_{inv} + \cancel{p}_T + \phi_{\ell\ell} + \text{b-tag}$ + (37), (39), (40), (42)	+ CJV on j_{decay} + (45)
$\chi_1^+ \chi_2^0 j$	no b	0.350 fb	0.013 fb	0.012 fb
$\chi_1^- \chi_2^0 j$	no b	0.168 fb	0.004 fb	0.004 fb
$\chi_2^0 \chi_2^0 j$	no b	0.012 fb	0.001 fb	< 0.001 fb
$\tilde{g} \chi_1^0 jj$	no b	0.038 fb	0.001 fb	< 0.001 fb
$\tilde{g} \chi_1^0 j$	no b	0.008 fb	$\ll 0.001$ fb	$\ll 0.001$ fb
$\chi_1^+ \chi_2^- jj$	no b	0.016 fb	< 0.001 fb	< 0.001 fb
$\chi_1^- \chi_2^+ jj$	no b	0.015 fb	< 0.001 fb	< 0.001 fb
$\chi_4^0 \chi_2^0 jj$	no b	0.013 fb	< 0.001 fb	< 0.001 fb
$\chi_2^+ \chi_2^0 jj$	no b	0.012 fb	< 0.001 fb	$\ll 0.001$ fb
$\chi_2^- \chi_2^0 jj$	no b	0.007 fb	< 0.001 fb	$\ll 0.001$ fb
\sum further processes		0.639 fb	< 0.024 fb	< 0.021 fb

Table 16: Total cross sections of further SUSY backgrounds to the VBF $h \rightarrow WW$ channel for average squark masses of 1.1 TeV.

masses is even more pronounced as even at high masses the dominant contributions come from the squark production with a t-channel gluino exchange ³, which also depends on the increased gluino mass. For the processes involving charginos the dominant contributions at low masses involve squarks, but a noticeable fraction of the electroweak gaugino pairs originate from virtual W or Z boson decay. As these contributions are independent from the squark mass, there is a noticeable fraction of the cross section which remains at higher squark masses. The slepton processes do not involve any squarks or gluinos and therefore stay independent of the mass variation.⁴

For average squark masses of 1.1 TeV (see column 2 of Tables 1 and 2) we checked the size of further SUSY contributions to see if the dominant processes at low squark masses are still the largest ones at higher squark masses. For the processes with not too tiny cross sections at low squark masses, the results are presented in Tables 15 and 16. Most of the other processes also have a reduced cross section at higher squark masses, therefore the processes with the largest cross sections are again within the list of the previously selected processes. One exception is the process $\chi_1^\pm \chi_2^0 j$, which shows a slightly increased cross section. This is due to interference effects between graphs with and without squarks. But still the overall contribution of this process to the SUSY background is only a few percent.

As the mass of the light neutral Higgs boson remains nearly unaffected by a variation of the first and second generation squark masses and the gluino mass, the cross section of the signal process $h \rightarrow WW$ remains unchanged. It is $\sigma = 2.91$ fb for the cuts in the left plot and $\sigma = 1.33$ fb for the ones of the right plot of Fig. 19.

For higher squark and gluino masses, the processes $\chi_1^\pm \chi_2^0 jj$ give the largest contributions to the SUSY backgrounds, at a total SUSY background level which is smaller by a factor of

$$S/B^{SUSY} = 6.2 \tag{50}$$

compared to the signal cross section.

6.2 Scenario SPS1a-slope

The scenario SPS1a-slope is characterized by SUSY particle masses which are about 30% higher compared to our default scenario SPS1amod (average $m_{\tilde{q}} = 703$ GeV, $m_{\chi_1^\pm} \approx m_{\chi_2^0} \approx 245$ GeV). The cross sections at this scenario are shown in Table 17. Most noteworthy is the behavior of the slepton contributions. They are not affected by the variation of gluino or squark mass, but here the 30% higher slepton masses lead to a reduction of the slepton contribution by 65% compared to the scenario SPS1amod.

The higher Higgs boson mass results in a higher signal cross section. Combined with the smaller backgrounds, the signal to background ratio increases strongly compared to SPS1amod.

³This holds for our approximation containing only $\alpha_s^2 \alpha^2$ -contributions as well as for the full process with all possible Feynman graphs.

⁴The slepton branching ratios change slightly due to higher-order corrected χ_1^\pm and χ_2^0 masses.

Processes	Cuts	basic + rap. gap Eqs. (35) + (36)	+ m_{inv} + \cancel{p}_T + $\phi_{\ell\ell}$ + b-tag + (37), (39), (40), (42)	+ CJV on j_{decay} + (45)
$\chi_1^+ \chi_1^- jj$	no b	0.60 fb	0.032 fb	0.032 fb
$\chi_1^+ \chi_1^- jj$	b-contr.	0.03 fb	0.002 fb	0.002 fb
$\chi_2^0 \chi_1^0 jj$	no b	0.25 fb	0.013 fb	0.013 fb
$\chi_2^0 \chi_1^0 jj$	b-contr.	0.03 fb	0.001 fb	0.001 fb
$\tilde{\ell}^+ \tilde{\ell}^- jj$	no b	0.81 fb	0.010 fb	0.010 fb
$\chi_1^+ \chi_2^0 jj$	no b	1.12 fb	0.069 fb	0.039 fb
$\chi_1^- \chi_2^0 jj$	no b	0.58 fb	0.040 fb	0.023 fb
$\chi_2^0 \chi_2^0 jj$	no b	0.39 fb	0.027 fb	0.011 fb
$\chi_2^0 \chi_2^0 jj$	b-contr.	0.03 fb	0.001 fb	0.001 fb
$\sum B^{SUSY}$		3.84 fb	0.195 fb	0.132 fb
VBF $h \rightarrow WW$		5.32 fb	2.37 fb	2.37 fb
S/B^{SUSY}		1.4	12	18

Table 17: Total cross sections of SUSY backgrounds dominant at low squark masses to the VBF $h \rightarrow WW$ channel for the scenario SPS1a-slope.

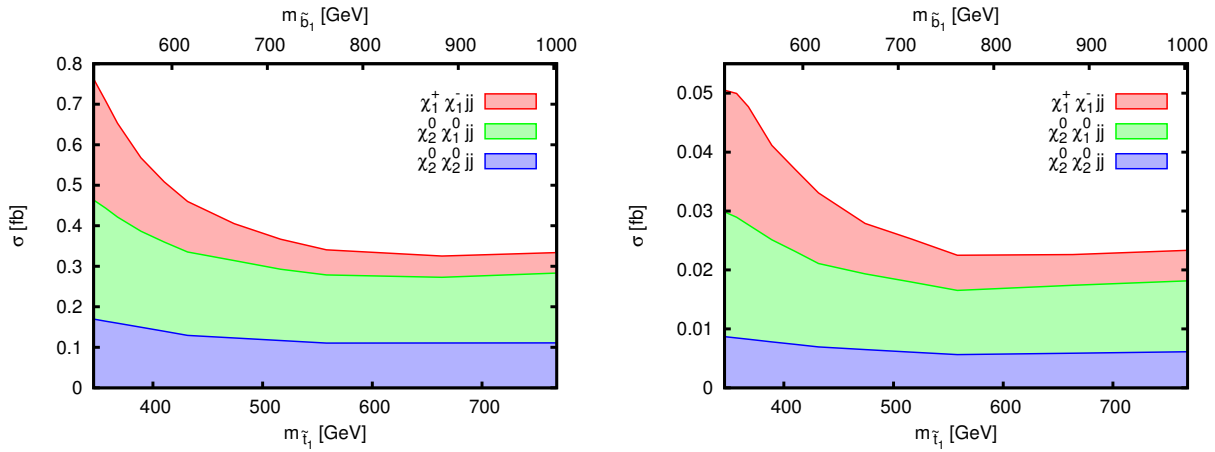


Figure 20: Third generation squark mass dependencies for the b-quark contributions of the SUSY-backgrounds as a function of the \tilde{t}_1 - mass. Left panel: with cuts from Eqs. (35) + (36). Right panel: with additional cuts from Eqs. (37), (39), (40) and (45).

6.3 Stop/Sbottom Mass Dependence of b-Quark Contributions

The b-quark contributions of the SUSY processes involve mostly third generation squarks. We therefore check the dependence on their mass by varying M_{q3L} , M_{tR} , M_{bR} , A_t , A_b and M_3 by a factor $(1 + \rho)$ with $0 \leq \rho \leq 1$.

At low \tilde{t}_1 masses, the chargino pair production is dominated by \tilde{t}_1 pair production. However, there are also small contributions from the production of heavy Higgs bosons with a subsequent decay into a chargino pair which remain as the only contributions for larger \tilde{t}_1 masses. The cross section as a function of the \tilde{t}_1 mass is shown in Fig. 20. The slight increase of the cross section at low masses on the right plot is due to the cut on the invariant jet pair mass, which is less efficient for larger masses.

For the next-to-lightest neutralino plus lightest neutralino production, the dependence on the \tilde{b}_1 mass is smaller, for reasons described in Sect. 4.2. At high \tilde{b}_1 masses, only the contributions from the heavy Higgs bosons remain (see Fig. 20). The slight increase above \tilde{b}_1 masses of 750 GeV is due to small changes in the mass of the heavy Higgs bosons and the next-to lightest neutralino which lead to minor changes to branching ratios. For the b-quark contributions of the production of a next-to lightest neutralino pair plus two jets the dominant contributions come from the same Feynman Graph topologies as in the $\chi_2^0 \chi_1^0 jj$ case. Therefore the mass dependence of both processes is much alike.

In this scenario series, the Higgs boson mass slightly increases from 118 GeV for $m_{\tilde{t}_1} = 345$ GeV up to 123 GeV for $m_{\tilde{t}_1} = 768$ GeV. This leads to an increased cross section for the $h \rightarrow WW$ signal process ranging from $\sigma = 1.33$ fb up to $\sigma = 1.98$ fb for the final set of cuts.

7 Contributions to the Background in other Scenarios

In this section, we investigate effects due to different sparticle masses which do change the characteristics of our scenario like branching ratios. More specifically, we consider a scenario with light sleptons at low and high squark masses for the dominant SUSY processes. For the process $\chi_1^+ \chi_1^- jj$ we also study the effect of a very light LSP as well as small mass differences of the particles within one cascade decay. Again, we do not conserve the mSUGRA assumptions.

7.1 Scenario with Light Selectrons and Smuons

7.1.1 Squark / Gluino Masses like in SPS1amod

In a scenario where χ_1^\pm and χ_2^0 are heavier than \tilde{e}_L and $\tilde{\mu}_L$ as well as lighter than $\tilde{\tau}_{1/2}$, the chargino and next-to-lightest neutralino will decay into \tilde{e}_L and $\tilde{\mu}_L$ instead of into $\tilde{\tau}$ leptons; the subsequent slepton decay will not produce a tau lepton, but an electron or muon, which can be detected directly.

These values for slepton masses (see Table 1) are obtained by lowering the soft SUSY breaking mass parameters M_{eL} and $M_{\mu L}$ at low energies from 194.4 GeV in SPS1amod to 134.4 GeV and increasing $M_{\tau L}$ from 193.6 GeV to 393.6 GeV as well as $M_{\tau R}$ from 133.4 GeV to 333.4 GeV. The other SUSY particle masses and parameters remain the same, leaving the signal processes $h \rightarrow \tau\tau$ and $h \rightarrow WW$ in vector boson fusion unaffected.

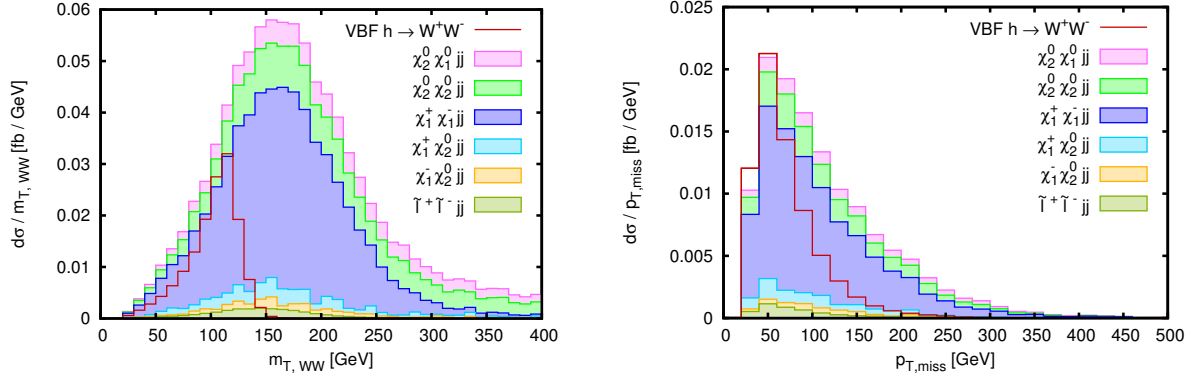


Figure 21: Transverse WW mass and \cancel{p}_T distributions analogous to Fig. 11, but for the scenario with light sleptons, including the slepton channel and the reducible SUSY background processes. B-quark contributions included where relevant.

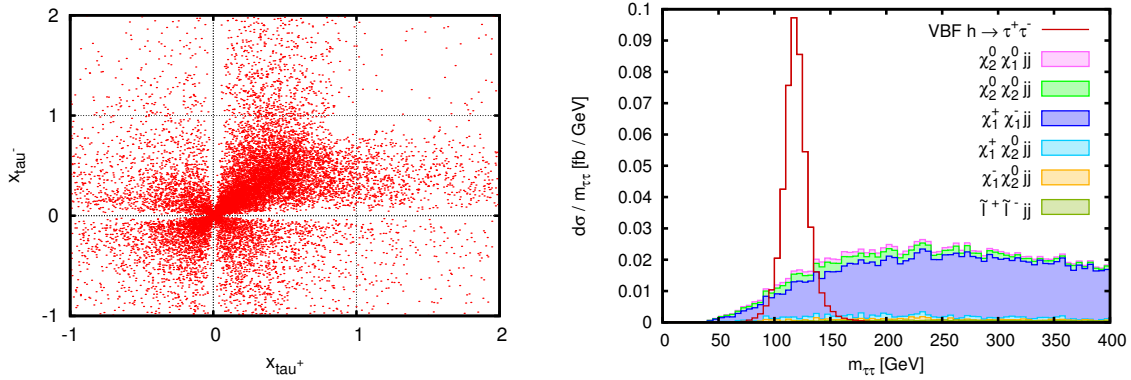


Figure 22: Left panel: tau momentum fractions for the chargino process, analogous to Fig. 9, but for the scenario with light sleptons. The right panel shows the reconstructed tau pair mass in this scenario with the same cuts as Fig. 10, including b-quark contributions, the slepton channel and the reducible SUSY background processes. The detector effects on the \cancel{p}_T measurement from Eq. (29) are taken into account in both plots.

The production cross sections for the processes involving electroweak gaugino pairs remain unchanged; the important effects show up in the decay chains. Looking at the electron and muon final states, we get an increased cross section by a factor of 8.3 before lepton cuts for the chargino process, which equals roughly $BR(\tau \rightarrow \ell \bar{\nu}_\ell \nu_\tau)^{-2}$, and accounts for the missing suppression factor corresponding to the leptonic τ decays. The effect on the decay chain of the next-to-lightest neutralino is quite different: As the masses of the sneutrinos are linked to the masses of the sleptons, they become light as well. Therefore a large fraction of the next-to-lightest neutralinos now decays completely invisibly, leading to a cross section only enhanced by a small factor of 1.6 for the $\chi_2^0 \chi_1^0 jj$ channel (including decays) compared to the SPS1amod scenario, again before lepton cuts.

The missing tau decay has further impact on distributions and cut efficiencies: Without the tau decay the charged final state leptons have larger transverse momenta and many more events pass the initial lepton cuts. The missing transverse momentum cut is not very efficient as well (Fig. 21), because there are less invisible particles in the final state. On the

other hand, the cut on the transverse WW mass is more efficient now, as can be seen in Fig. 21. So after all cuts, the cross section for the chargino process is increased by a factor of 15, while the next-to-lightest neutralino contributions remain the same.

The $\tilde{\ell}^+ \tilde{\ell}^- jj$ channel is increased by about a factor of two to three with respect to the SPS1amod scenario due to the lighter \tilde{e}_L and $\tilde{\mu}_L$ and due to the fact that these sleptons now always decay to an electron or muon and the LSP. The minor $\tilde{\tau}$ contributions become even smaller than in the SPS1amod scenario.

The situation for the reducible background is completely different for the light sleptons of the first and second generation. Beforehand, we had a large amount of soft jets and leptons from tau decays as additional particles which could easily be missed by the detector. Now, as the stau leptons are heavy, we have additional hard electrons and muons and no tau jets instead of the tau lepton decay products. As a first consequence, all processes that required a tau jet as tagging jet ($\chi_1^\pm \chi_2^0 j$ and $\chi_2^0 \chi_2^0(j)$) give no contribution. Also the veto on additional hard jets from the SUSY particle decays has no effect. The process $\chi_1^\pm \chi_2^0 jj$ shows a reduced contribution due to the additional hard leptons. The only process that is enhanced in this scenario is $\chi_2^0 \chi_2^0 jj$. Here the invisible decay modes of χ_2^0 play an important role in mimicking the signature of the signal process.

Altogether, the total signal to background ratio for the $h \rightarrow WW$ signal reduces by more than a factor of two to

$$S/B^{SUSY} = 0.69 \quad (51)$$

compared to $S/B^{SUSY} = 1.9$ in the SPS1amod scenario. Detailed numbers are given in Table 18.

Processes	Cuts	basic + rap. gap Eqs. (35) + (36)	+ m_{inv} + \cancel{p}_T + $\phi_{\ell\ell}$ + b-tag + (37), (39), (40), (42)	+ CJV on j_{decay} + (45)
$\chi_1^+ \chi_1^- jj$	no b	36.0 fb	1.09 fb	1.09 fb
$\chi_1^+ \chi_1^- jj$	b-contr.	12.5 fb	0.14 fb	0.14 fb
$\chi_2^0 \chi_1^0 jj$	no b	2.38 fb	0.103 fb	0.103 fb
$\chi_2^0 \chi_1^0 jj$	b-contr.	0.72 fb	0.020 fb	0.020 fb
$\tilde{\ell}^+ \tilde{\ell}^- jj$	no b	2.77 fb	0.082 fb	0.082 fb
$\chi_1^+ \chi_2^0 jj$	no b	2.00 fb	0.133 fb	0.133 fb
$\chi_1^- \chi_2^0 jj$	no b	0.97 fb	0.052 fb	0.051 fb
$\chi_2^0 \chi_2^0 jj$	no b	4.92 fb	0.267 fb	0.267 fb
$\chi_2^0 \chi_2^0 jj$	b-contr.	0.59 fb	0.023 fb	0.023 fb
$\sum B^{SUSY}$		62.9 fb	1.91 fb	1.91 fb
VBF $h \rightarrow WW$		2.91 fb	1.32 fb	1.32 fb
S/B^{SUSY}		0.046	0.69	0.69

Table 18: Total cross sections of SUSY backgrounds dominant at low squark masses to the VBF $h \rightarrow WW$ channel for the scenario with light sleptons.

For the $h \rightarrow \tau\tau$ signal process, in this scenario, the background also increases significantly, especially the $\chi_1^+ \chi_1^- jj$ contribution due to the previously mentioned reasons. However, the tau pair mass reconstruction is still very efficient in reducing the SUSY background processes. The signal to background ratio with all cuts and detector effects on the missing transverse momentum measurement is $S/B^{SUSY} = 4.3$, compared to $S/B^{SUSY} = 12$ for SPS1amod, including b-quark contributions. The background is quite flat in the reconstructed tau pair mass, allowing for an effective subtraction from a sideband analysis, see Fig. 22.

7.1.2 Higher Squark and Gluino Masses

We have seen in the last subsection that light sleptons can increase the SUSY background cross sections substantially. As the numbers above were produced for relatively light squark masses, we now want to check the size of the SUSY background processes with higher squark and gluino masses, combined with these light selectrons and smuons. Therefore we take the SUSY breaking parameters from the scenario discussed in the last subsection, and increase the values for $M_{q_1L}, M_{q_2L}, M_{uR}, M_{dR}, M_{cR}, M_{sR}, M_{q_3L}, M_{tR}, M_{bR}, A_t, A_b$ and M_3 by a factor of 2. This leads to squark and gluino masses like in the second column of Table 1, and stop and sbottom mass values like in the third column. As the stop masses increase, the Higgs boson mass is shifted to a value of 123 GeV, leading to higher values for the $h \rightarrow WW$ signal process. As expected from the mass behavior discussed in Section 6, the processes involving charginos and neutralinos are reduced by at least a factor of two, leading to a

Processes	Cuts	basic + rap. gap Eqs. (35) + (36)	+ $m_{inv} + \cancel{p}_T + \phi_{\ell\ell}$ + b-tag + (37), (39), (40), (42)	+ CJV on j_{decay} + (45)
$\chi_1^+ \chi_1^- jj$	no b	11.79 fb	0.266 fb	0.266 fb
$\chi_1^+ \chi_1^- jj$	b-contr.	2.43 fb	0.040 fb	0.040 fb
$\chi_2^0 \chi_1^0 jj$	no b	0.069 fb	0.001 fb	0.001 fb
$\chi_2^0 \chi_1^0 jj$	b-contr.	0.473 fb	0.011 fb	0.011 fb
$\tilde{\ell}^+ \tilde{\ell}^- jj$	no b	2.78 fb	0.086 fb	0.086 fb
$\chi_1^+ \chi_2^0 jj$	no b	1.08 fb	0.058 fb	0.058 fb
$\chi_1^- \chi_2^0 jj$	no b	0.47 fb	0.019 fb	0.019 fb
$\chi_2^0 \chi_2^0 jj$	no b	0.48 fb	0.018 fb	0.018 fb
$\chi_2^0 \chi_2^0 jj$	b-contr.	0.40 fb	0.014 fb	0.014 fb
$\sum B^{SUSY}$		19.97 fb	0.513 fb	0.513 fb
VBF $h \rightarrow WW$		4.50 fb	2.00 fb	2.00 fb
S/B^{SUSY}		0.23	3.9	3.9

Table 19: Total cross sections of SUSY backgrounds dominant at low squark masses to the VBF $h \rightarrow WW$ channel for the scenario with light sleptons but higher squark and gluino masses.

signal to background ratio of

$$S/B^{SUSY} = 3.9 \quad (52)$$

after all cuts. Numbers at different cut levels are given in Table 19.

7.2 Scenario with Light LSP

Next we address the question whether the backgrounds increase substantially when increasing the available phase space for the decay leptons, especially in context of the tau pair mass reconstruction. We modify the mass values for some decay products in the output from the spectrum generator. This is then again fed into SDECAY [25] for the branching ratio calculation. While we do not have a genuine MSSM model anymore, we still can use it to investigate some characteristics. We want to focus on the chargino decay, starting from the scenario SPS1amod. The chargino can decay in two possible ways:

$$\begin{aligned} \chi_1^\pm &\rightarrow \tilde{\tau}^\pm \nu \rightarrow \tau^\pm \chi_1^0 \nu, \\ \chi_1^\pm &\rightarrow W^\pm \chi_1^0 \rightarrow \ell^\pm \chi_1^0 \nu. \end{aligned} \quad (53)$$

When we change $m_{\tilde{\tau}}$ from 133 GeV to 100 GeV and $m_{\chi_1^0}$ from 98 GeV to 1 GeV, there is roughly 80 GeV available for kinematics at each step.

As shown in Fig. 23, we get harder leptons as expected, and thus more events pass the transverse momentum cut on the leptons. Depending on the cuts, this results in factors up to 1.8 on the cross section. For the final cuts of the $h \rightarrow WW$ analysis, this factor is 1.4. There is no strong enhancement of the background when the cuts of $h \rightarrow \tau\tau$ after mass reconstruction are applied, as can be seen on the right plot of Fig. 23. For the $h \rightarrow \tau\tau$ channel, the ratio of lepton and missing transverse momentum in the scenario with light sleptons is more signal like than in the scenario of this section.

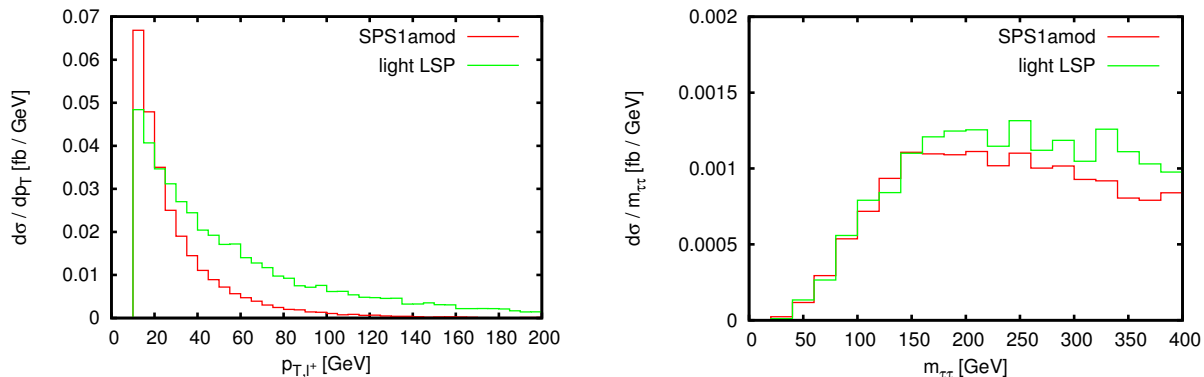


Figure 23: Left panel: p_{T,ℓ^+} distribution of $\chi_1^+ \chi_1^- jj$ with cuts (30) - (32). Right panel: reconstructed invariant tau pair mass with the additional cuts on x_i and $\cos \phi_{\ell\ell}$ from Eq. (33).

7.3 Scenario with Small Mass Differences in the Decay Chain

In this SPS1a-like scenario with the unified trilinear coupling A_0 shifted from -100 GeV to -750 GeV, we can see the effect of a very small mass difference of only 9 GeV between the

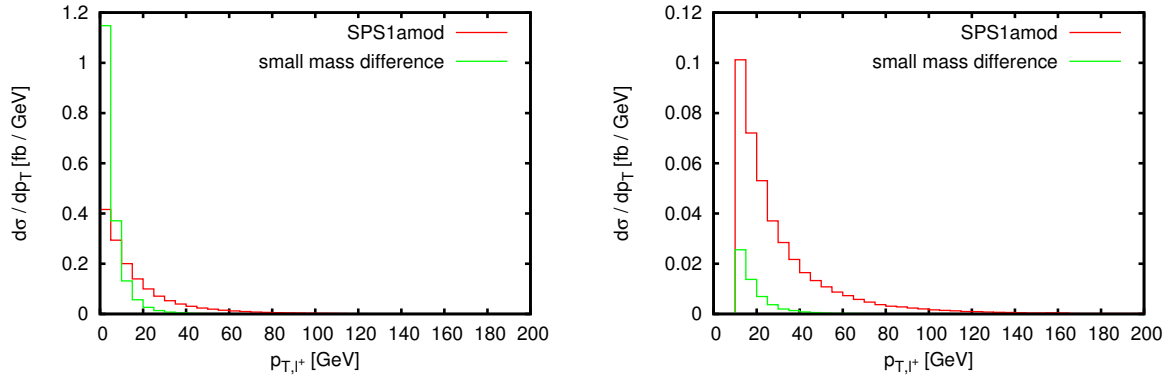


Figure 24: p_T distribution for positively charged lepton in a scenario with a small difference between the $\tilde{\tau}_1$ and χ_1^0 mass. In the left plot, otherwise generated with the cuts from Eqs. (30)+(31), also the region $p_{T,\ell} < 10$ GeV is shown.

masses of the tau slepton and the LSP on the chargino decay chain. As, in this scenario, the decay of the chargino into a tau slepton is dominant, we actually probe the effects of this mass difference on the distributions of the $\chi_1^+ \chi_1^- jj$ channel.

As depicted in Fig. 24, the transverse momentum of the tau lepton is very small, and the cut on the lepton transverse momentum of 10 GeV removes most of the chargino contributions. If we compare this with the results for SPS1amod and the scenario with a light LSP, we find that a $\tilde{\tau}_1 - \chi_1^0$ mass difference of about 10 GeV leads to negligible cross sections while the 36 GeV from SPS1amod results in cross section values where further cuts are necessary for the suppression of the background. If we increase this difference even more as in the light LSP scenario of Sect. 7.2, the additional effect is much smaller.

8 LHC with 7 TeV Center of Mass Energy

So far we have shown results for the LHC at 14 TeV center of mass energy, as, due to the small signal cross sections, the Higgs boson searches via the VBF topology are more relevant for higher center of mass energies; a detailed analysis of Higgs boson production in vector boson fusion will need of order 30 fb^{-1} or more of integrated luminosity at 14 TeV center of mass energy. But as the LHC performs very well with 7 TeV so far, we give some results on SUSY backgrounds to VBF Higgs production at 7 TeV as well.

8.1 Scenario SPS1amod

At first, the results for our base scenario SPS1amod are shown. As one can see in Fig. 25 and Table 20, the SUSY background processes have a much stronger dependence on the center of mass energy than the Higgs boson production in vector boson fusion, as they involve much heavier particles. Hence the signal to background ratio for the signal channel $h \rightarrow WW$ improves by about a factor of 2, yielding

$$S/B^{SUSY} = 3.6. \quad (54)$$

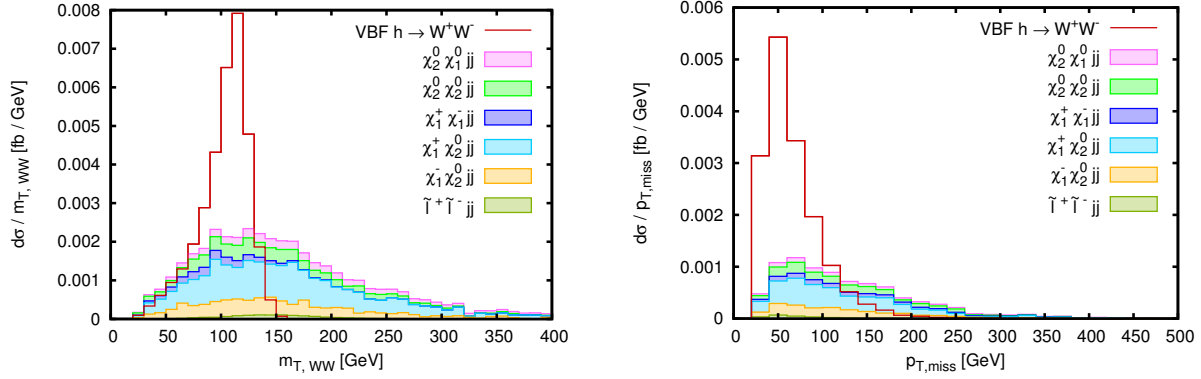


Figure 25: Left panel: Transverse WW mass distribution with cuts (35) - (37). Right panel: p_T distribution with cuts (35) - (37), (39). For both plots the scenario SPS1amod at 7 TeV center of mass energy is assumed and b-quark contributions are included.

Processes	Cuts	basic + rap. gap Eqs. (35) + (36)	+ m_{inv} + p_T + $\phi_{\ell\ell}$ + b-tag + (37), (39), (40), (42)	+ CJV on j_{decay} + (45)
$\chi_1^+ \chi_1^- jj$	no b	145 ab	9.9 ab	9.9 ab
$\chi_1^+ \chi_1^- jj$	b-contr.	26 ab	0.6 ab	0.6 ab
$\chi_2^0 \chi_1^0 jj$	no b	99 ab	8.9 ab	8.9 ab
$\chi_2^0 \chi_1^0 jj$	b-contr.	24 ab	0.9 ab	0.9 ab
$\tilde{\ell}^+ \tilde{\ell}^- jj$	no b	206 ab	4.4 ab	4.4 ab
$\chi_1^+ \chi_2^0 jj$	no b	588 ab	53.7 ab	36.5 ab
$\chi_1^- \chi_2^0 jj$	no b	246 ab	24.8 ab	16.5 ab
$\chi_2^0 \chi_2^0 jj$	no b	158 ab	20.2 ab	8.8 ab
$\chi_2^0 \chi_2^0 jj$	b-contr.	13 ab	0.6 ab	0.3 ab
$\sum B^{SUSY}$		1505 ab	124 ab	86.8 ab
VBF $h \rightarrow WW$		777 ab	316 ab	316 ab
S/B^{SUSY}		0.52	2.5	3.6

Table 20: Total cross sections of SUSY backgrounds to the VBF $h \rightarrow WW$ channel for the scenario SPS1amod at 7 TeV center of mass energy.

This signal to background ratio is an upper limit calculated in a scenario with very light squark and gluino masses. For a center of mass energy of 14 TeV we found a reduction by a factor of 3.3 when considering more realistic values of squark and gluino masses of the first two generations. Assuming a reduction of the same order at 7 TeV, the SUSY backgrounds would mean no harm. Furthermore the central jet veto used to suppress additional jets from decayed SUSY particles also vetoes additional jets from QCD radiation which occur more frequently in the SUSY processes than in the signal process (see Sect. 4.2.3).

8.2 Scenario with Heavier \tilde{q} / \tilde{g} and Light \tilde{e} / $\tilde{\mu}$

Finally we show results for the scenario from Section 7.1.2, which incorporates the higher cross sections of the SUSY background processes together with squark masses that fit better to current exclusion limits of the CMSSM parameter space by ATLAS [10] and CMS [11]. As depicted in Fig. 26 and Table 21, we get an improvement in the signal to background ratio by roughly a factor of 2 compared to 14 TeV center of mass energy, like for the scenario SPS1amod. Therefore the SUSY background processes account for 12% of the signal cross section for $h \rightarrow WW$ in this optimized scenario. As the dominant SUSY processes in this scenario do not lead to additional jets from SUSY particle decays, a central jet veto would only reduce jets originating from additional QCD radiation.

In this scenario the Standard Model like Higgs boson mass is assumed to be 123 GeV and therefore close to the value where ATLAS and CMS have seen an excess in their Standard Model Higgs boson searches [49, 50]. If we set up a model like SPS1amod2 introduced in Section 2, but increase the SUSY breaking terms for the first and second generation squarks according to $\xi = 1.5$ (corresponds to an average squark mass of 1.3 TeV) we increase the Higgs boson mass to $m_h = 124.3$ GeV. This raises the signal cross section with all cuts to $\sigma^{h \rightarrow WW} = 527$ ab. With light sleptons of the first and second generation the background processes account for $\sigma^{SUSY} = 63$ ab leading to roughly the same signal to background ratio

$$S/B^{SUSY} = 8.4. \quad (55)$$

The situation for the $h \rightarrow \tau\tau$ signal process is again very comfortable. With all cuts discussed for this channel and taking detector effects on the missing transverse momentum measurement into account, we get $S/B^{SUSY} = 43$, with a signal cross section of 340 ab for the scenario with a Higgs boson mass of 123 GeV.

9 Summary and Conclusions

We have investigated SUSY induced background processes to the production of the light Higgs boson in the MSSM via vector boson fusion at leading order accuracy. Particularly, we discussed dominant background contributions to the Higgs boson decays into tau leptons and W bosons for fully leptonic final states for a SPS1a-like scenario and scenarios with partly changed characteristics with respect to the SPS1a-like one.

Our analysis was split into two parts: First we searched for processes that match the signal signature exactly and therefore contribute to the irreducible background. In this class the two production processes $\chi_1^+ \chi_1^- jj$ and $\chi_2^0 \chi_1^0 jj$ with subsequent decays of χ_1^\pm

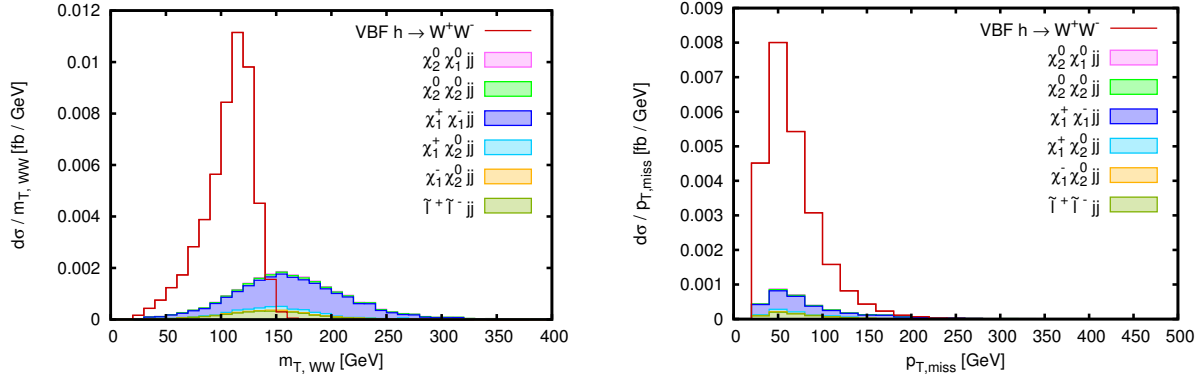


Figure 26: Left panel: Transverse WW mass distribution with cuts (35) - (37). Right panel: \cancel{p}_T distribution with cuts (35) - (37), (39). For both plots, the scenario with light sleptons and higher squark/gluino masses at 7 TeV center of mass energy is assumed and b-quark contributions included.

Processes	Cuts	basic + rap. gap Eqs. (35) + (36)	+ m_{inv} + \cancel{p}_T + $\phi_{\ell\ell}$ + b-tag + (37), (39), (40), (42)	+ CJV on j_{decay} + (45)
$\chi_1^+ \chi_1^- jj$	no b	1756 ab	35.0 ab	35.0 ab
$\chi_1^+ \chi_1^- jj$	b-contr.	216 ab	2.2 ab	2.2 ab
$\chi_2^0 \chi_1^0 jj$	no b	1.6 ab	0.03 ab	0.03 ab
$\chi_2^0 \chi_1^0 jj$	b-contr.	43 ab	0.7 ab	0.7 ab
$\tilde{\ell}^+ \tilde{\ell}^- jj$	no b	482 ab	13.4 ab	13.4 ab
$\chi_1^+ \chi_2^0 jj$	no b	132 ab	3.8 ab	3.8 ab
$\chi_1^- \chi_2^0 jj$	no b	48 ab	1.3 ab	1.3 ab
$\chi_2^0 \chi_2^0 jj$	no b	32 ab	1.7 ab	1.7 ab
$\chi_2^0 \chi_2^0 jj$	b-contr.	35 ab	0.8 ab	0.8 ab
$\sum B^{SUSY}$		2746 ab	58.9 ab	58.9 ab
VBF $h \rightarrow WW$		1193 ab	476 ab	476 ab
S/B^{SUSY}		0.44	8.1	8.1

Table 21: Total cross sections of SUSY backgrounds to the VBF $h \rightarrow WW$ channel for the scenario with light sleptons and higher squark/gluino masses at 7 TeV center of mass energy.

and χ_2^0 have been found to give the largest SUSY backgrounds to the mentioned leptonic signatures of the Higgs boson. The contributions with b-quarks in the final state have been checked separately; though sizable if only basic cuts are applied, taking into account the complete set of cuts, including a b-jet veto, reduces these b-quark related background processes sufficiently. We estimated the effect of a central jet veto on these processes and showed that the veto can lead to a further reduction of the SUSY background. Smaller irreducible background contributions come from the $\tilde{\ell}^+ \tilde{\ell}^- jj$ production.

The processes $\chi_1^\pm \chi_2^0 jj$ and $\chi_2^0 \chi_2^0 jj$ contribute to the reducible background, as they lead to additional jets or leptons from the decay of the SUSY particles. Even with a central jet veto these contributions are twice as large as the irreducible SUSY background in SPS1a-like scenarios.

Starting from the SPS1a-like scenario, we have shown the SUSY background cross section dependence on the squark and gluino masses for mass values roughly between 550 GeV and 1.6 TeV. The SUSY background decreases with increasing squark and gluino masses and is lowered by 70% for squark masses of 1.1 TeV. For higher masses the SUSY contributions remain constant. We also checked a scenario where the selectrons and smuons are the lightest sleptons, which leads to significantly larger backgrounds.

For the $h \rightarrow \tau\tau$ signal, we saw that the reconstruction of the invariant tau pair mass, which is possible in the collinear approximation of tau lepton decays, is very efficient in reducing the cross sections of the SUSY background processes. For the SPS1a-like scenario the backgrounds after mass reconstruction and a mass window cut around the Higgs boson mass are more than one order of magnitude smaller than the signal. Even for the scenario with light sleptons and squarks as light as in SPS1a, the SUSY background processes account for not more than 23% of the signal cross section.

SUSY backgrounds to the $h \rightarrow WW$ channel are a bit more troublesome. They are under sufficient control for the SPS1a-like scenario with a ratio $S/B^{SUSY} = 1.9$ after passing all cuts. With larger squark masses the SUSY background rates decrease substantially. However, for the scenario with light sleptons and SPS1a-like squarks, the background can be larger than the signal. With higher squark masses of around 1.1 TeV, which are still in agreement with current measurements from ATLAS and CMS, a ratio $S/B^{SUSY} = 3.9$ remains.

These numbers have been calculated for the LHC operating at 14 TeV center of mass energy, as Higgs boson production in vector boson fusion is mainly targeted at this energy. The analysis for the 7 TeV LHC shows that the cross sections of our SUSY background processes decrease about twice as much as the ones from the signal processes.

Overall, we could confirm that VBF Higgs boson production with a subsequent decay into tau leptons is a very clean signal, not only in the Standard Model but also in the MSSM. Considering the subsequent decay into W bosons, particularly with an additional \cancel{p}_T -cut, the SUSY background processes are mostly under control for squark and gluino masses at or above the current exclusion limits from the LHC.

Acknowledgments

We would like to thank Stefan Gieseke, Simon Plätzer, Christian Röhr and Peter Richardson for discussions and **Herwig++** support and Jürgen Reuter and Christian Speckner for helping with the **Whizard** comparison and Margarete Mühlleitner for answering questions concerning decays of SUSY particles and **SUSYHIT**. We gratefully acknowledge helpful discussions with Sophy Palmer, Eva Popena and Michael Rauch. The Feynman diagrams were done using JaxoDraw [51]. This work was supported by the BMBF under Grant No. 05H09VKG (“Verbundprojekt HEP-Theorie”) and by the Initiative and Networking Fund of the Helmholtz Association, contract HA-101 (“Physics at the Terascale”).

References

- [1] **CMS Collaboration**, G. L. Bayatian *et al.*, *J.Phys. G* **34** (2007) 995–1579.
- [2] **The ATLAS Collaboration**, G. Aad *et al.*, [arXiv:0901.0512 \[hep-ex\]](#).
- [3] T. Plehn, D. L. Rainwater and D. Zeppenfeld, *Phys.Lett.* **B454** (1999) 297–303, [arXiv:hep-ph/9902434](#).
- [4] A. Datta, A. Djouadi, M. Guchait and F. Moortgat, *Nucl.Phys.* **B681** (2004) 31–64, [arXiv:hep-ph/0303095](#).
- [5] M. Consonni, *Nucl.Phys.Proc.Suppl.* **177-178** (2008) 271–272.
- [6] H. Baer, V. Barger and G. Shaughnessy, *Phys.Rev.* **D78** (2008) 095009, [arXiv:0806.3745 \[hep-ph\]](#).
- [7] **ATLAS Collaboration**, *Phys.Lett.* **B705** (2011) 174–192, [arXiv:1107.5003 \[hep-ex\]](#).
- [8] **CMS Collaboration**, S. Chatrchyan *et al.*, *Phys. Rev. Lett.* **106** (2011) 231801, [arXiv:1104.1619 \[hep-ex\]](#);
CMS Collaboration, CMS-PAS-HIG-11-009, (2011).
- [9] M. Duhrssen, S. Heinemeyer, H. Logan, D. Rainwater, G. Weiglein and D. Zeppenfeld, *Phys.Rev.* **D70** (2004) 113009, [arXiv:hep-ph/0406323](#).
- [10] **ATLAS Collaboration**, G. Aad *et al.*, *Phys.Lett.* **B701** (2011) 186–203, [arXiv:1102.5290 \[hep-ex\]](#);
ATLAS Collaboration, G. Aad *et al.*, *Eur.Phys.J.* **C71** (2011) 1682, [arXiv:1103.6214 \[hep-ex\]](#);
ATLAS Collaboration, I.Vivarelli, talk given at EPS HEP 2011, Grenoble, France.
- [11] **CMS Collaboration**, S. Chatrchyan *et al.*, *JHEP* **1106** (2011) 026, [arXiv:1103.1348 \[hep-ex\]](#);
CMS Collaboration, S. Chatrchyan *et al.*, *JHEP* **1108** (2011) 155, [arXiv:1106.4503 \[hep-ex\]](#);
CMS Collaboration, CMS-PAS-SUS-11-003, (2011).

- [12] T. Han, G. Valencia and S. Willenbrock, *Phys.Rev.Lett.* **69** (1992) 3274–3277, [arXiv:hep-ph/9206246](#);
M. Spira, *Fortsch.Phys.* **46** (1998) 203–284, [arXiv:hep-ph/9705337](#);
T. Figy, C. Oleari and D. Zeppenfeld, *Phys.Rev.* **D68** (2003) 073005, [arXiv:hep-ph/0306109](#);
E. L. Berger and J. M. Campbell, *Phys.Rev.* **D70** (2004) 073011, [arXiv:hep-ph/0403194](#).
- [13] M. Ciccolini, A. Denner and S. Dittmaier, *Phys.Rev.Lett.* **99** (2007) 161803, [arXiv:0707.0381 \[hep-ph\]](#);
M. Ciccolini, A. Denner and S. Dittmaier, *Phys.Rev.* **D77** (2008) 013002, [arXiv:0710.4749 \[hep-ph\]](#).
- [14] T. Figy, S. Palmer and G. Weiglein, *JHEP* **1202** (2012) 105, [arXiv:1012.4789 \[hep-ph\]](#).
- [15] R. V. Harlander, J. Vollinga and M. M. Weber, *Phys.Rev.* **D77** (2008) 053010, [arXiv:0801.3355 \[hep-ph\]](#).
- [16] A. Bredenstein, K. Hagiwara and B. Jager, *Phys.Rev.* **D77** (2008) 073004, [arXiv:0801.4231 \[hep-ph\]](#);
J. Andersen, T. Binoth, G. Heinrich and J. Smillie, *JHEP* **0802** (2008) 057, [arXiv:0709.3513 \[hep-ph\]](#).
- [17] P. Bolzoni, F. Maltoni, S.-O. Moch and M. Zaro, *Phys.Rev.Lett.* **105** (2010) 011801, [arXiv:1003.4451 \[hep-ph\]](#).
- [18] A. Djouadi and M. Spira, *Phys.Rev.* **D62** (2000) 014004, [arXiv:hep-ph/9912476](#).
- [19] W. Hollik, T. Plehn, M. Rauch and H. Rzehak, *Phys.Rev.Lett.* **102** (2009) 091802, [arXiv:0804.2676 \[hep-ph\]](#).
- [20] B. C. Allanach *et al.*, *Eur.Phys.J.* **C25** (2002) 113–123, [arXiv:hep-ph/0202233](#).
- [21] M. S. Carena, S. Heinemeyer, C. E. M. Wagner and G. Weiglein, [arXiv:hep-ph/9912223](#).
- [22] D. L. Rainwater, D. Zeppenfeld and K. Hagiwara, *Phys.Rev.* **D59** (1998) 014037, [arXiv:hep-ph/9808468](#).
- [23] N. Kauer, T. Plehn, D. L. Rainwater and D. Zeppenfeld, *Phys.Lett.* **B503** (2001) 113–120, [arXiv:hep-ph/0012351](#).
- [24] A. Djouadi, M. M. Muhlleitner and M. Spira, *Acta Phys.Polon.* **B38** (2007) 635–644, [arXiv:hep-ph/0609292](#).
- [25] M. Muhlleitner, A. Djouadi and Y. Mambrini, *Comput.Phys.Commun.* **168** (2005) 46–70, [arXiv:hep-ph/0311167](#).

- [26] A. Djouadi, J.-L. Kneur and G. Moultaka, *Comput.Phys.Commun.* **176** (2007) 426–455, [arXiv:hep-ph/0211331](#).
- [27] A. Djouadi, J. Kalinowski and M. Spira, *Comput.Phys.Commun.* **108** (1998) 56–74, [arXiv:hep-ph/9704448](#).
- [28] W. Porod, *Comput.Phys.Commun.* **153** (2003) 275–315, [arXiv:hep-ph/0301101](#).
- [29] S. Heinemeyer, W. Hollik and G. Weiglein, *Comput.Phys.Commun.* **124** (2000) 76–89, [arXiv:hep-ph/9812320](#);
S. Heinemeyer, W. Hollik and G. Weiglein, *Eur.Phys.J.* **C9** (1999) 343–366, [arXiv:hep-ph/9812472](#);
G. Degrassi, S. Heinemeyer, W. Hollik, P. Slavich and G. Weiglein, *Eur.Phys.J.* **C28** (2003) 133–143, [arXiv:hep-ph/0212020](#);
M. Frank, T. Hahn, S. Heinemeyer, W. Hollik, H. Rzehak and G. Weiglein, *JHEP* **0702** (2007) 047, [arXiv:hep-ph/0611326](#).
- [30] P. Z. Skands *et al.*, *JHEP* **0407** (2004) 036, [arXiv:hep-ph/0311123](#);
B. C. Allanach *et al.*, *Comput.Phys.Commun.* **180** (2009) 8–25, [arXiv:0801.0045 \[hep-ph\]](#).
- [31] **Tevatron Electroweak Working Group, CDF and D0 Collaboration**, E. Brubaker *et al.*, [arXiv:hep-ex/0603039](#).
- [32] J. Alwall *et al.*, *JHEP* **0709** (2007) 028, [arXiv:0706.2334 \[hep-ph\]](#).
- [33] J. Alwall, M. Herquet, F. Maltoni, O. Mattelaer and T. Stelzer, *JHEP* **1106** (2011) 128, [arXiv:1106.0522 \[hep-ph\]](#).
- [34] J. Pumplin *et al.*, *JHEP* **0207** (2002) 012, [arXiv:hep-ph/0201195](#).
- [35] W. Kilian, T. Ohl and J. Reuter, *Eur.Phys.J.* **C71** (2011) 1742, [arXiv:0708.4233 \[hep-ph\]](#);
M. Moretti, T. Ohl and J. Reuter, [arXiv:hep-ph/0102195 \[hep-ph\]](#).
- [36] W. Beenakker, R. Hopker, M. Spira and P. Zerwas, *Nucl.Phys.* **B492** (1997) 51–103, [arXiv:hep-ph/9610490 \[hep-ph\]](#).
- [37] W. Beenakker, M. Klasen, M. Kramer, T. Plehn, M. Spira *et al.*, *Phys.Rev.Lett.* **83** (1999) 3780–3783, [arXiv:hep-ph/9906298 \[hep-ph\]](#).
- [38] M. Bahr *et al.*, *Eur.Phys.J.* **C58** (2008) 639–707, [arXiv:0803.0883 \[hep-ph\]](#).
- [39] J. Alwall *et al.*, *Comput.Phys.Commun.* **176** (2007) 300–304, [arXiv:hep-ph/0609017](#).
- [40] P. Richardson, *JHEP* **0111** (2001) 029, [arXiv:hep-ph/0110108](#).
- [41] K. Arnold *et al.*, *Comput.Phys.Commun.* **180** (2009) 1661–1670, [arXiv:0811.4559 \[hep-ph\]](#);
K. Arnold *et al.*, [arXiv:1107.4038 \[hep-ph\]](#).

- [42] **ATLAS Collaboration**, D. W. Miller, ATL-PHYS-PROC-2010-049, (2010).
- [43] **ATLAS Collaboration**, G. Aad *et al.*, *New J.Phys.* **13** (2011) 053033, [arXiv:1012.5104 \[hep-ex\]](#).
- [44] D. L. Rainwater and D. Zeppenfeld, *Phys.Rev.* **D60** (1999) 113004, [arXiv:hep-ph/9906218](#).
- [45] R. K. Ellis, I. Hinchliffe, M. Soldate and J. J. V. D. Bij, *Nuclear Physics B* **297** (1988) 221 – 243.
- [46] D. L. Rainwater, R. Szalapski and D. Zeppenfeld, *Phys.Rev.* **D54** (1996) 6680–6689, [arXiv:hep-ph/9605444](#);
D. L. Rainwater, D. Summers and D. Zeppenfeld, *Phys.Rev.* **D55** (1997) 5681–5684, [arXiv:hep-ph/9612320](#).
- [47] **CMS Collaboration**, CMS-PAS-BTV-09-001, (2009);
CMS Collaboration, CMS-PAS-BTV-10-001, (2010).
- [48] M. Cacciari, G. P. Salam and G. Soyez, *JHEP* **0804** (2008) 063, [arXiv:0802.1189 \[hep-ph\]](#).
- [49] **ATLAS Collaboration**, ATLAS-CONF-2011-163, (2011).
- [50] **CMS Collaboration**, CMS-PAS-HIG-11-032, (2011).
- [51] D. Binosi and L. Theussl, *Comput.Phys.Commun.* **161** (2004) 76–86, [arXiv:hep-ph/0309015](#);
D. Binosi, J. Collins, C. Kaufhold and L. Theussl, *Comput.Phys.Commun.* **180** (2009) 1709–1715, [arXiv:0811.4113 \[hep-ph\]](#);
J. A. M. Vermaseren, *Comput.Phys.Commun.* **83** (1994) 45–58.